Linking YAP to Müller Glia Quiescence Exit in the Degenerative Retina

Annaïg Hamon, Diana García-García, Divya Ail, Juliette Bitard, Albert Chesneau, Deniz Dalkara, Morgane Locker, Jérôme E. Roger, Muriel Perron

Article

Cell Reports

Linking YAP to Müller Glia Quiescence Exit in the Degenerative Retina

Graphical Abstract

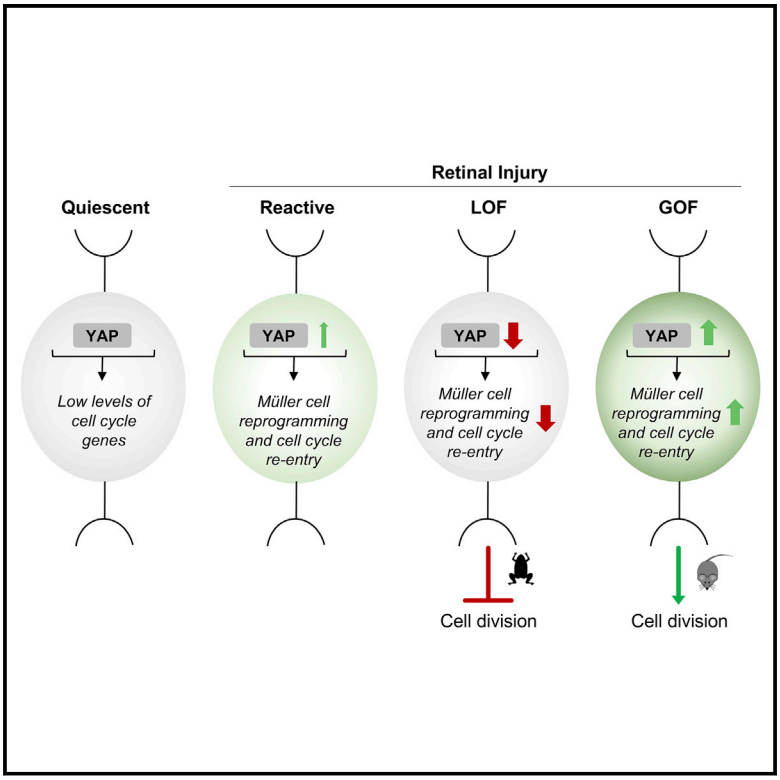

Authors

Annaïg Hamon, Diana García-García, Divya Ail, ..., Morgane Locker, Jérôme E. Roger, Muriel Perron

Correspondence

jerome.roger@u-psud.fr (J.E.R.), muriel.perron@u-psud.fr (M.P.)

In Brief

While fish and amphibian Müller cells behave as retinal stem cells upon injury, their regenerative potential is limited in mammals. Hamon et al. show that YAP is required for their cell-cycle re-entry in *Xenopus* and is sufficient in mouse to awake them from quiescence and trigger their proliferative response.

Highlights

- YAP is required for *Xenopus* Müller glia proliferation in response to injury
- YAP is required for mouse Müller glia exit from quiescence upon degeneration
- YAP5SA reprograms mouse Müller glia into highly proliferative cells
- YAP functionally interacts with EGFR signaling in Müller cells

Hamon et al., 2019, Cell Reports *27*, 1712–1725
May 7, 2019
https://doi.org/10.1016/j.celrep.2019.04.045

CellPress

OPEN ACCESS
CellPress

Cell Reports
Article

Linking YAP to Müller Glia Quiescence Exit in the Degenerative Retina

Annaïg Hamon,[1,3] Diana García-García,[1,3] Divya Ail,[1,3] Juliette Bitard,[1] Albert Chesneau,[1] Deniz Dalkara,[2] Morgane Locker,[1] Jérôme E. Roger,[1,*] and Muriel Perron[1,4,*]

[1]Paris-Saclay Institute of Neuroscience, CERTO-Retina France, CNRS, Univ Paris Sud, Université Paris-Saclay, Orsay 91405, France
[2]Sorbonne Université, UPMC Univ Paris 06, INSERM, CNRS, Institut de la Vision, Paris, France
[3]These authors contributed equally
[4]Lead Contact
*Correspondence: jerome.roger@u-psud.fr (J.E.R.), muriel.perron@u-psud.fr (M.P.)
https://doi.org/10.1016/j.celrep.2019.04.045

SUMMARY

Contrasting with fish or amphibian, retinal regeneration from Müller glia is largely limited in mammals. In our quest toward the identification of molecular cues that may boost their stemness potential, we investigated the involvement of the Hippo pathway effector YAP (Yes-associated protein), which is upregulated in Müller cells following retinal injury. Conditional *Yap* deletion in mouse Müller cells prevents cell-cycle gene upregulation that normally accompanies reactive gliosis upon photoreceptor cell death. We further show that, in *Xenopus*, a species endowed with efficient regenerative capacity, YAP is required for their injury-dependent proliferative response. In the mouse retina, where Müller cells do not spontaneously proliferate, YAP overactivation is sufficient to induce their reprogramming into highly proliferative cells. Overall, we unravel a pivotal role for YAP in tuning Müller cell proliferative response to injury and highlight a YAP-EGFR (epidermal growth factor receptor) axis by which Müller cells exit their quiescence state, a critical step toward regeneration.

INTRODUCTION

Neurodegenerative retinal diseases, such as retinitis pigmentosa or age-related macular degeneration, ultimately lead to vision loss, as a consequence of photoreceptor cell death. Driving retinal self-repair from endogenous neural stem cells in patients represents an attractive therapeutic strategy. Among cellular sources of interest are Müller cells, the major glial cell type in the retina (Bringmann et al., 2006). In certain species, such as zebrafish or *Xenopus*, they behave as genuine stem cells, endowed with the ability to reprogram into a progenitor-like state upon retinal damage, proliferate, and regenerate lost photoreceptors (Hamon et al., 2016; Langhe et al., 2017; Wan and Goldman, 2016). In mammals, however, their proliferative response to injury is extremely limited. Following acute retinal damage, mouse Müller glial cells rapidly re-enter the G1 phase of the cell cycle, as inferred by increased *cyclin* gene expression, but they rarely divide (Dyer and Cepko, 2000). Suggesting that they nonetheless retain remnants of repair capacities, their proliferation and neurogenic potential can be stimulated, by supplying exogenous growth factors such as heparin-binding epidermal growth factor (EGF)-like growth factor (HB-EGF), by overexpressing the proneural gene *Ascl1a*, or via cell fusion with Wnt-activated transplanted stem cells (Hamon et al., 2016; Jorstad et al., 2017; Sanges et al., 2016; Ueki et al., 2015; Wilken and Reh, 2016). Our understanding of the genetic and signaling network sustaining Müller cell stemness potential is, however, far from being complete. Identifying novel molecular cues is thus of utmost importance to foresee putative candidates that could be targeted for regenerative medicine. We here investigated whether the Hippo pathway effector YAP might influence Müller cell reactivation and how it would intersect with other critical signaling pathways.

The Hippo pathway is a kinase cascade that converges toward two terminal effectors, YAP (Yes-associated protein) and TAZ (transcriptional coactivator with PDZ-binding motif). Both are transcriptional coactivators of TEAD family transcription factors. The Hippo pathway emerged as a key signaling in a wide range of biological processes (Fu et al., 2017), including stem cell biology (Barry and Camargo, 2013; Mo et al., 2014). Of note, it proved to be dispensable under physiological conditions in some adult stem cells, such as mammary gland, pancreatic, intestinal, and importantly, neural stem cells (Azzolin et al., 2014; Chen et al., 2014a; Huang et al., 2016; Zhang et al., 2014). It can nonetheless become essential under pathological conditions, as described, for example, in the context of intestinal regeneration following injury (Barry et al., 2013; Gregorieff et al., 2015). YAP status in adult neural tissue repair has hitherto never been investigated. We recently discovered that YAP and TEAD1 are specifically expressed in murine Müller cells, and that their expression and activity are enhanced upon retinal damage (Hamon et al., 2017). We thus sought to determine whether YAP could be required for injury-induced Müller glia reactivation. We found in mouse that YAP triggers cell-cycle gene upregulation in Müller glial cells following photoreceptor cell death. In line with the idea of a conserved role in Müller cell-cycle re-entry, blocking YAP function in *Xenopus* results in a dramatically reduced proliferative response following acute retinal damage or photoreceptor cell ablation. Finally, we report that the limited proliferative response of murine Müller glia can be circumvented

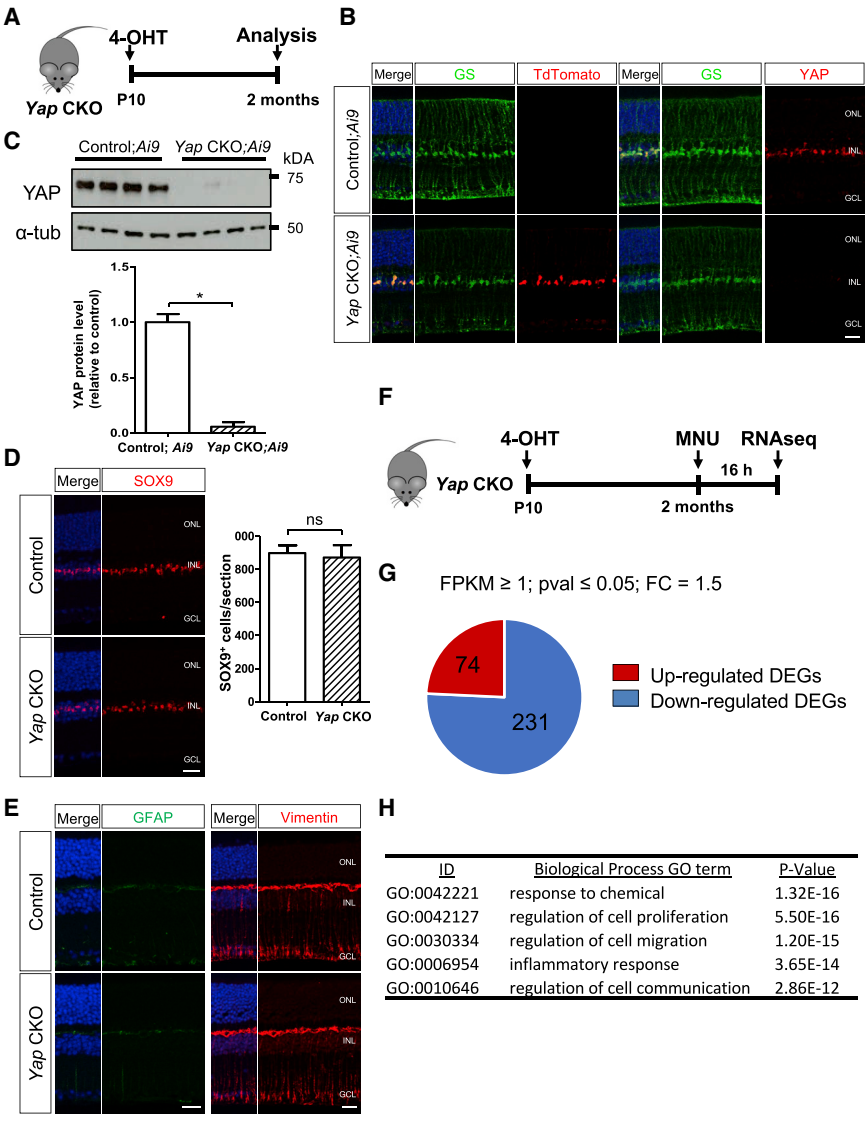

ID	Biological Process GO term	P-Value
GO:0042221	response to chemical	1.32E-16
GO:0042127	regulation of cell proliferation	5.50E-16
GO:0030334	regulation of cell migration	1.20E-15
GO:0006954	inflammatory response	3.65E-14
GO:0010646	regulation of cell communication	2.86E-12

Figure 1. *Yap* CKO Retinas Exhibit Altered Transcriptional Response to Injury

(A) Timeline diagram of the experimental procedure used in (B–E). $Yap^{flox/flox}$ mice with or without the *Ai9* reporter allele (control or control;*Ai9*) and $Yap^{flox/flox}$;*Rax-CreER*^{T2} mice with or without the *Ai9* reporter allele (*Yap* CKO or *Yap* CKO;*Ai9*) received a single dose of 4-OHT at P10 and were analyzed at P60.

(B) Retinal sections immunostained for TdTomato, glutamine synthetase (GS; a Müller cell marker), or YAP.

(C) Western blot analysis of YAP expression on retinal extracts. α-Tubulin labeling was used to normalize the signal. n = 4 mice for each condition.

(D) Retinal sections immunostained for SOX9. n = 3 mice for each condition.

(E) Retinal sections immunostained for GFAP or Vimentin.

(F) Timeline diagram of the experimental procedure used in (G) and (H). $Yap^{flox/flox}$ (control) and $Yap^{flox/flox}$;*Rax-CreER*^{T2} (*Yap* CKO) mice received a single dose of 4-OHT at P10 and a single dose of MNU at 2 months. Retinas were then subjected to RNA-sequencing 16 h later.

(G) Pie chart representing the number of DEGs found to be upregulated or downregulated in MNU-injected *Yap* CKO retinas compared with MNU-injected control ones.

(H) Results of Gene Ontology (GO) enrichment analysis exemplifying six over-represented GO biological processes related to retinal response to injury.

In (B), (D), and (E), nuclei were counterstained with DAPI (blue). Mann-Whitney test, *p ≤ 0.05. All results are reported as mean ± SEM. Scale bars, 20 μm. GCL, ganglion cell layer; INL, inner nuclear layer; ns, non-significant; ONL, outer nuclear layer. See also Figures S1 and S2 and Table S1.

and significantly enhanced by YAP overexpression. We further show such YAP mitogenic function relies on its interplay with epidermal growth factor receptor (EGFR) signaling. As a whole, this study highlights the critical role of YAP in driving Müller cells to exit quiescence and thus reveals a potential target for regenerative medicine.

RESULTS

Yap Conditional Knockout in Mouse Müller Cells Does Not Compromise Their Maintenance under Physiological Conditions

To investigate the role of YAP in murine Müller glia, we generated a $Yap^{flox/flox}$; *Rax-CreER*^{T2} mouse line allowing for Cre-mediated conditional gene ablation specifically in Müller cells (Pak et al., 2014; Reginensi et al., 2013). It is thereafter named *Yap* CKO (conditional knockout), whereas "control" refers to $Yap^{flox/flox}$ mice. *Yap* deletion was induced in fully differentiated Müller cells, through 4-hydroxytamoxifen (4-OHT) intraperitoneal injection at postnatal day (P) 10 (Figure 1A). Phenotypic analyses were then conducted on 2-month-old mice. We first confirmed Müller cell-specific *Cre* expression and *Yap* deletion efficiency in *Yap* CKO mice carrying the Rosa26-CAG-lox-stop-lox-TdTomato reporter (*Ai9*) transgene (Figures 1B and 1C). We next wondered whether expression of TAZ (the second effector of the Hippo pathway) could be increased in our model and thus potentially compensate for *Yap* deletion, as previously reported in mammalian cell lines (Finch-Edmondson et al., 2015). In these physiological conditions, TAZ protein level was actually similar in *Yap* CKO and control mice (Figure S1A), suggesting an absence of compensatory mechanisms. Finally, we assessed global retinal organization and function in *Yap* CKO mice. Immunostaining for various retinal neuron markers and electroretinogram (ERG) recordings under scotopic and photopic conditions revealed neither structural nor functional difference compared with control retinas (Figures S1B–S1D). Müller cells, whose identity was assessed with Sox9 labeling, were also normally distributed (Figure 1D). They did not display any sign of stress

reactivity, as inferred by the expression of intermediate filament proteins, glial fibrillary acidic protein (GFAP), and Vimentin (Figure 1E). Taken together, these results demonstrate that lack of YAP expression in Müller cells from P10 does not impact the overall retinal structure, neuron and glia maintenance, nor the visual function in 2-month-old mice.

Yap Deletion Impairs Mouse Müller Cell Reactivation upon Photoreceptor Degeneration

We next investigated YAP function in a degenerative context. Retinal degeneration was triggered in *Yap* CKO mice through *in vivo* methylnitrosourea (MNU) injections, a well-established paradigm for inducible photoreceptor cell death (Chen et al., 2014b). In order to evaluate the impact of *Yap* deletion on Müller glia early response to injury, all of the analyses were performed 16 h after MNU injection, at the onset of photoreceptor cell death (Figures 1F and S2A). As previously described (Hamon et al., 2017), YAP protein expression level was upregulated in wild-type (WT) retinas upon MNU injection, and as expected, we found it effectively decreased in our MNU-injected *Yap* CKO model (Figure S2B). In contrast with the physiological situation, this was accompanied by a compensatory increase of TAZ levels (Figure S2C). Yet, this enhanced expression is likely insufficient to entirely compensate for the loss of YAP activity, as inferred by the downregulation of *Cyr61*, a well-known YAP/TAZ target gene (Lai et al., 2011; Figure S2D). We next assessed GFAP expression as a marker of reactive gliosis upon MNU injection. Interestingly, we found it increased at both the mRNA and protein levels in *Yap* CKO mice compared with control ones, reflecting a potential higher degree of retinal stress (Figures S2E and S2F). This led us to further investigate the molecular impact of *Yap* deletion in reactive Müller cells, through a large-scale transcriptomic analysis comparing non-injected WT mice, MNU-injected control mice, and MNU-injected *Yap* CKO mice. This allowed identifying 305 differentially expressed genes (DEGs), 75% of them being downregulated in MNU-injected *Yap* CKO retinas compared with MNU-injected control ones (Figure 1G; Table S1). The top-enriched biological processes they belong to include "response to chemical," "regulation of cell proliferation," and "inflammatory response." This strongly suggests that lack of YAP expression profoundly alters Müller cell transcriptional response to retinal injury (Figure 1H).

Yap Knockout Prevents Cell-Cycle Gene Upregulation in Mouse Reactive Müller Cells

As we were seeking for a potential function of YAP in Müller cell reactivation, we focused our interest on identified genes related to the GO group "regulation of cell proliferation." *Z* score-based hierarchical clustering for the 70 corresponding DEGs revealed three distinct clusters (Figure S3A). One particularly caught our attention because the 52 DEGs it contains appear less responsive to injury in the absence of YAP. These are indeed: (1) expressed at very low levels in wild-type mice, (2) strongly upregulated in MNU-injected control mice, (3) while being only moderately enriched in MNU-injected *Yap* CKO mice. This is the case, for instance, of four cell-cycle regulator coding genes, *Ccnd1*, *Ccnd2*, *Ccnd3*, and *Cdk6* (Figure 2A). Further validation was conducted by qPCR, immunostaining, and western blot for Cyclin D1 and Cyclin D3, which are specifically expressed in Müller cells. This confirmed their downregulation upon MNU injection in *Yap* CKO mice compared with controls (Figures 2B–2D). Noticeably, we found that the pluripotent leukemia inhibitory factor (LIF) and the reprogramming factor Klf4 follow the same profile, suggesting that the reprogramming process that initiates along with Müller cell-reactive gliosis is also impaired by *Yap* loss of function (Figure S3B).

To strengthen our results in a model closer to human retinal disease, we generated *Yap* CKO;*rd10* mice by breeding the *Yap* CKO line into the *rd10* background (*Pde6b*^{rd10} line, a model of retinitis pigmentosa) (Chang et al., 2007; McLaughlin et al., 1995). We next assessed Cyclin D1 and Cyclin D3 expression at P20 (Figures S4A and S4B), which corresponds to the period of intense rod cell death in *rd10* mice (Chang et al., 2007). As observed with the MNU model, protein levels for both cyclins were increased in Müller cells upon photoreceptor degeneration, and this upregulation was impaired in *Yap* CKO retinas. Taken together, these results demonstrate YAP involvement in the injury-induced transcriptional activation of cell-cycle genes, which likely reflects its role in pushing Müller cells out of their quiescent state. Of note, a YAP-dependent control of Cyclin D1 and D3 expression was also observed in physiological conditions (Figures S4C and S4D), suggesting that YAP regulates the basal level of cell-cycle genes in quiescent Müller cells as well.

Inhibition of YAP Prevents Müller Glia Proliferation upon Acute Retinal Damage or Selective Photoreceptor Cell Ablation in *Xenopus laevis*

All of the above results converge to the idea that YAP triggers cell-cycle re-entry of quiescent Müller glia upon injury. Because this process is not complete in murine Müller cells (they reactivate G1 phase genes but rarely divide), we turned to the frog to strengthen our hypothesis. *Xenopus* is an animal model endowed with regenerative capacity, in which Müller cells efficiently respond to injury by intense proliferation (Langhe et al., 2017). We first confirmed that, within the *Xenopus* central neural retina, YAP expression is restricted to Müller cells (Figure 3A) (Cabochette et al., 2015), as observed in mouse. We next sought to assess the impact of YAP inhibition by taking advantage of a *Xenopus laevis* transgenic line, hereafter named *Tg(dnYAP)*, in which a heat shock promoter (Hsp70) drives the expression of a dominant-negative YAP variant (Hayashi et al., 2014a; Nishioka et al., 2009; Figures 3B, S5A, and S5B). We first verified that heat-shocked *Tg(dnYAP)* embryos displayed a small eye phenotype, as previously demonstrated following *Yap*-Morpholino injection (Cabochette et al., 2015). Moreover, we found that this defective eye growth could be rescued by overexpressing an inducible and constitutively active form of YAP, YAPS98A-GR (Figures S5C–S5E). At latter developmental stages, two YAP target genes, *Ctgf* (connective tissue growth factor) and *Cyr61*, were downregulated in *Tg(dnYAP)* tadpole retinas upon heat-shock induction (Figure S5F). Altogether, these results validated the efficacy and specificity of dnYAP in inhibiting endogenous YAP function. We next assayed Müller cell proliferative response in a model of stab injury (Figure 3C). Importantly, we previously demonstrated that a majority of proliferating cells found at the injury site are indeed Müller cells

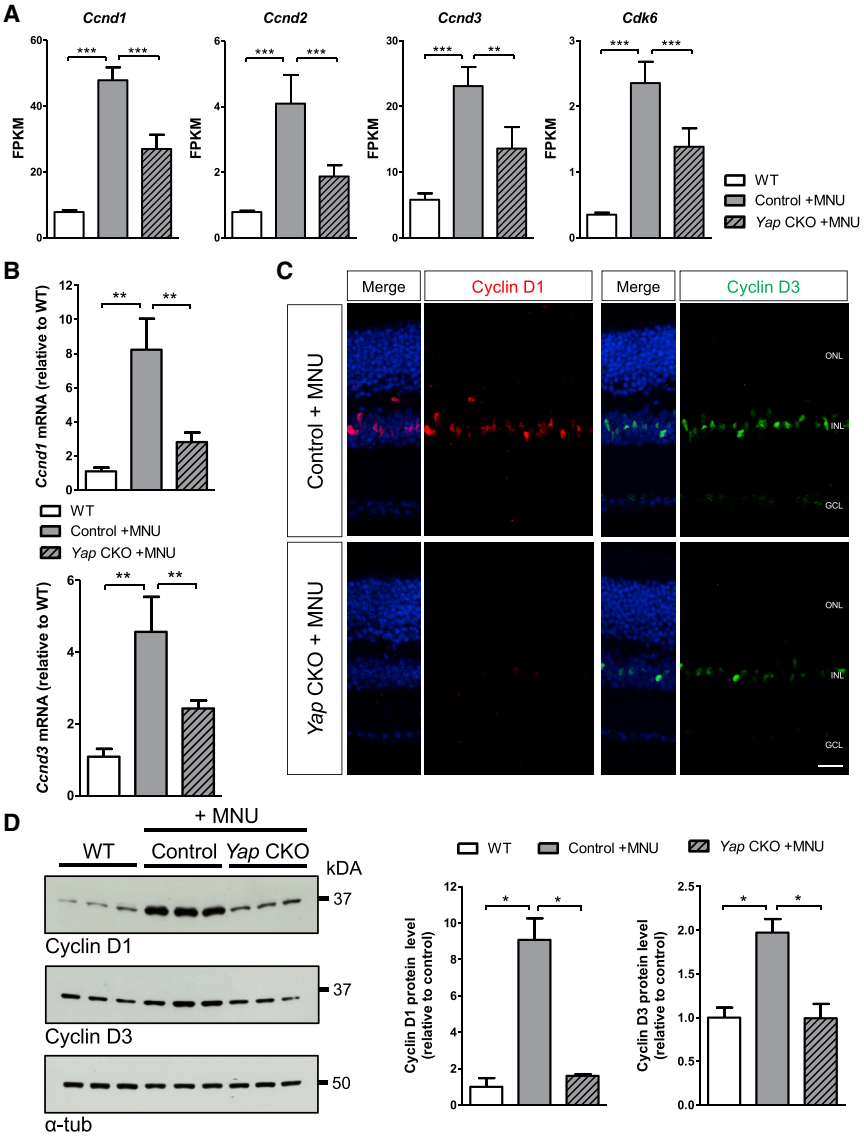

Figure 2. Cell-Cycle Gene Upregulation in Response to MNU Injection Is Compromised in *Yap* CKO Retinas

(A) Relative RNA expression (in fragments per kilobase of exon per million fragments mapped [FPKM]; data retrieved from the RNA-seq experiment) of *Ccnd1*, *Ccnd2*, *Ccnd3*, and *Cdk6* in retinas from non-injected WT mice or control and *Yap* CKO mice injected with 4-OHT and MNU as shown in Figure 1F.

(B) qRT-PCR analysis of *Ccnd1* and *Ccnd3* expression in the same experimental conditions (at least five biological replicates per condition were used).

(C) Retinal sections from control and *Yap* CKO mice, immunostained for Cyclin D1 or D3. Nuclei are counterstained with DAPI (blue).

(D) Western blot analysis of Cyclin D1 and D3 expression on retinal extracts from WT, control, and *Yap* CKO mice. α-Tubulin labeling was used to normalize the signal. n = 3 mice for each condition. Mann-Whitney test (except in A where p values were obtained using EdgeR), *p ≤ 0.05, **p ≤ 0.01; ***p ≤ 0.001. Scale bar: 20 μm. GCL, ganglion cell layer; INL, inner nuclear layer; ONL, outer nuclear layer. See also Figures S3 and S4.

(Langhe et al., 2017). Comparison of 5-bromo-2′-deoxyuridine (BrdU) incorporation in heat-shocked and non-heat-shocked wild-type retinas confirmed that heat shock does not affect proliferation by itself (Figure 3D). In contrast, the number of BrdU-labeled cells at the injury site was reduced by about 60% in heat-shocked *Tg(dnYAP)* tadpole retinas compared with controls (non-heat-shocked transgenic animals or heat-shocked non-transgenic siblings; Figure 3D). Of note, loss of YAP activity did not affect Müller cell density (Figure S5G), ruling out the possibility that defective BrdU incorporation might be due to an impaired cell survival. Finally, YAP requirement for Müller glia proliferative response to stab injury could be confirmed at post-metamorphic stage in froglets, with *Tg(dnYAP)* retinas exhibiting a reduction of 80% of BrdU-positive cells compared with controls (Figures 3E and 3F).

We next sought to reinforce these data in a model closer to the mouse MNU or *rd10* paradigms. In this purpose, we turned to a *Xenopus laevis* transgenic line that we previously established, allowing for conditional selective rod cell ablation (Langhe et al., 2017) [*Tg(Rho:GFP-NTR)*, hereafter named *Tg(NTR)*] (Figure 4A). This transgenic line expresses the nitroreductase (*NTR*) gene under the control of the *Rhodopsin* promoter, and photoreceptor degeneration can be induced by adding the enzyme ligand metronidazole (MTZ) to the tadpole rearing medium. Here again, we previously showed that about 80% of cells that proliferate upon rod cell ablation are indeed Müller cells (Langhe et al., 2017). The *Tg(dnYAP)* and *Tg(NTR)* lines were crossed to generate double-transgenic animals, in which inhibition of YAP can be triggered by heat shock, and photoreceptor degeneration by MTZ treatment (Figure 4B). As observed above with the stab injury, Müller cell proliferative response to rod cell death was dramatically reduced in double *Tg(dnYAP;NTR)* froglet retinas compared with *Tg(NTR)* control ones (Figure 4C). Altogether, although we cannot completely rule out the possibility of dnYAP off-target effects on Müller cell behavior, these data strongly support the idea that in different lesional contexts, YAP is required for *Xenopus* Müller glia cell-cycle re-entry and proliferation.

Forced YAP Expression in Mouse Müller Glial Cells Stimulates Their Proliferation Both *Ex Vivo* and *In Vivo*

Based on the above data on *Xenopus*, we next wondered whether mouse Müller cell inability to proliferate upon injury (despite cell-cycle gene reactivation) might be linked to insufficient levels

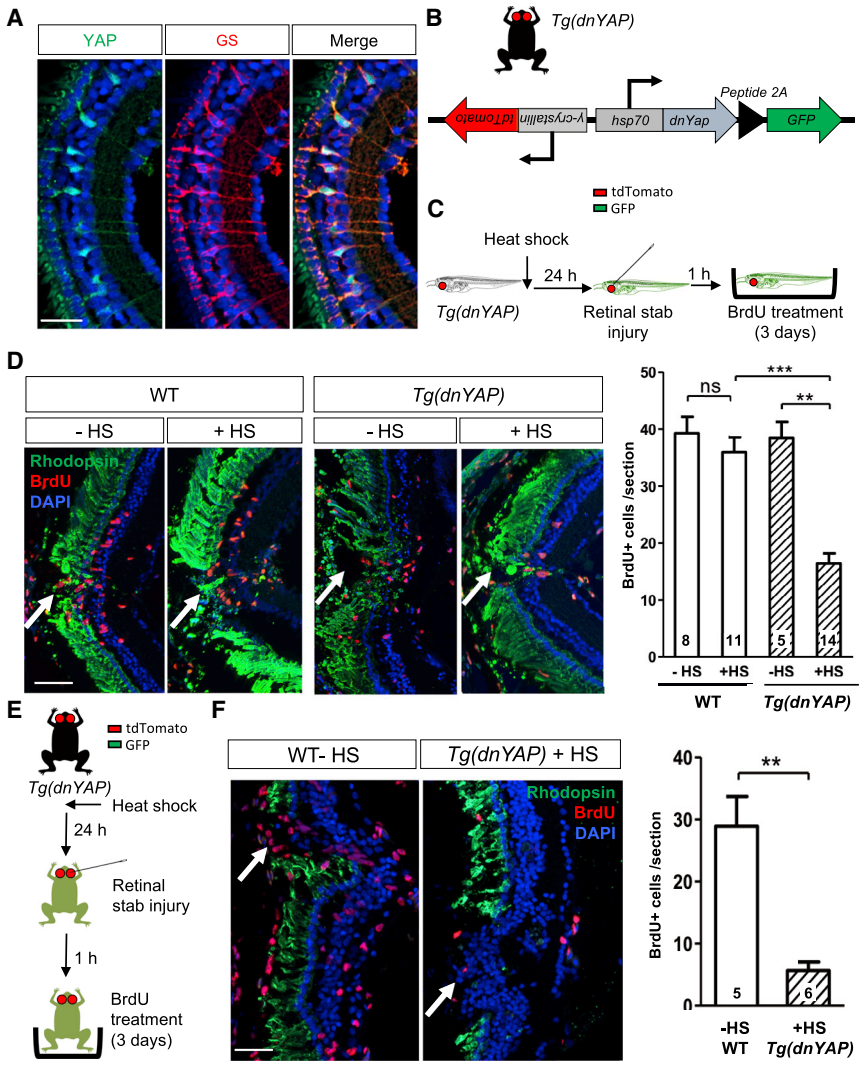

Figure 3. Inhibiting YAP Activity in *Xenopus* Reduces the Proliferative Retinal Response to a Stab Injury

(A) Retinal section from a stage 45 WT *Xenopus laevis* tadpole, immunostained for YAP and glutamine synthetase (GS; a marker of Müller cells). Nuclei are counterstained with Hoechst (blue).

(B) Schematic representation of the heat-shock-inducible dominant-negative *Yap* transgene (*dnYap*). *Tg(dnYAP)* transgenic animals can be selected based on tdTomato expression in the lens (driven by the γ-crystallin promoter). Heat-shocked efficiency can be assessed through GFP expression.

(C and E) Timeline diagrams of the experimental procedures used in (D) and (F), respectively. WT or *Tg(dnYAP)* pre-metamorphic tadpoles (stage 54–58; D) or froglets (stage 61–66; F) were heat-shocked, injured in the retina 24 h later, and transferred 1 h post-lesion in a BrdU solution for 3 more days.

(D and F) Retinal sections from animals that were heat-shocked (+HS) or not (−HS), immunostained for rhodopsin and BrdU. Nuclei are counterstained with DAPI (blue). Arrows point to the injury site. The number of retinas tested for each condition is indicated on the corresponding bar. Mann-Whitney test, $^{**}p \leq 0.01$, $^{***}p \leq 0.001$. All results are reported as mean ± SEM. Scale bars, 25 μm (A), 50 μm (D and F). ns, non-significant. See also Figure S5.

of YAP activity. To investigate this hypothesis, we decided to overexpress in mouse Müller cells a FLAG-tagged mutated YAP protein, YAP5SA, which is insensitive to Hippo pathway-mediated cytoplasmic retention (Zhao et al., 2007). To deliver this constitutively active form of YAP, we took advantage of an adeno-associated virus (AAV) variant, ShH10, which selectively targets Müller cells (Klimczak et al., 2009; Figures 5A and S6A–S6C). We then started by infecting retinal explants, a spontaneous model of retinal degeneration (Müller et al., 2017). We first found that levels of Cyclin D1 were significantly increased upon AAV-YAP5SA transduction compared with that of AAV-GFP-infected controls (Figures 5B and 5C). We next analyzed Müller cell proliferative activity through an EdU incorporation assay. In explants overexpressing YAP5SA, EdU labeling was strongly enhanced, with numerous patches containing a high density of EdU-positive cells (Figure 5D) found in regions with the highest infected cell density (as assessed by FLAG immunostaining; data not shown). Further quantitative analyses within the explant inner nuclear layer revealed that after a 7-day culture: (1) about 50% of YAP5SA-expressing cells were EdU labeled (Figures S6D and S6E), (2) the great majority (more than 88%) of EdU-positive cells were Müller cells (as inferred by their Sox9 labeling and their position; Figures S6F and S6G), and (3) up to ~25% of Müller cells were proliferating in AAV-YAP5SA-infected explants (Figure 5E). Of note, after such a 7-day culture, EdU-positive cells were mainly found in the explant periphery, where neurons are presumably more prone to degenerate (more exposed than those in the center). Importantly, however, after longer culture time period (12 days instead of 7), proliferation spread into the whole infected explant, and the percentage of EdU-labeled Müller cells then reached more than 75% (Figure 5F).

We next assessed the mitogenic potential of YAP5SA *in vivo*, following intravitreal AAV injection in adult mice (Figures 5G and 5H). Only rare proliferative cells were observed in control retinas. In contrast, many EdU-positive cells were found in retinas transduced with AAV-YAP5SA. Co-labeling with glutamine synthetase or SOX9 on retinal sections confirmed that a majority of these had a Müller cell identity (Figure S7A and data not shown). YAP5SA can thus trigger Müller glia cell-cycle re-entry *in vivo*. Altogether, these data reveal that YAP overactivation is sufficient to override the dormancy of murine Müller glial cells and boost their proliferative potential. Additionally, as shown in Figures S7B and S7C, increased expression of *Ascl1* was observed

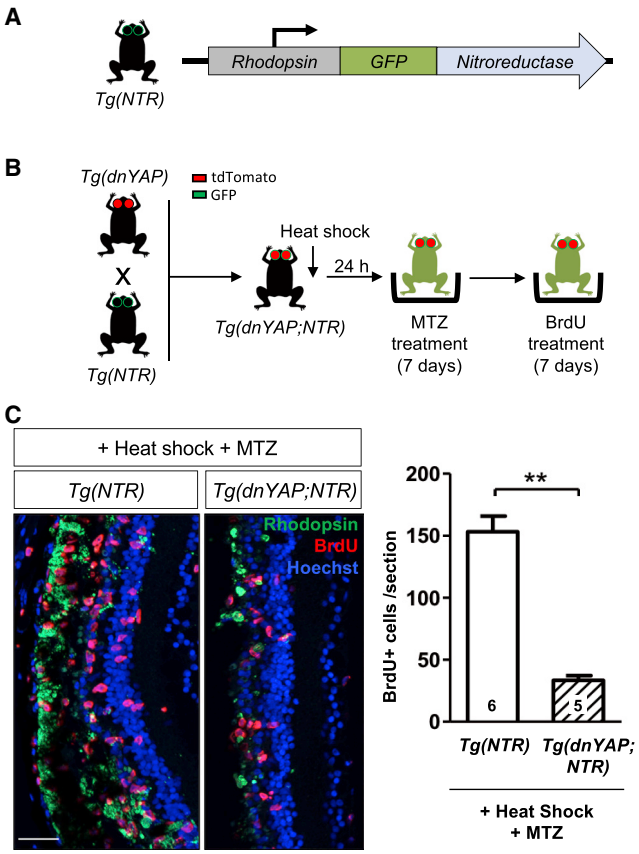

Figure 4. Inhibiting YAP Activity in *Xenopus* Reduces the Proliferative Retinal Response to Photoreceptor Degeneration

(A) Schematic representation of the transgene carried by the *Tg(NTR)* line. Transgenic animals can be selected based on GFP expression in rod cells (driven by the *Rhodopsin* promoter).

(B) Timeline diagram of the experimental procedures used in (C). *Tg(dnYAP)* were crossed with *Tg(NTR)* to generate double-transgenic *Tg(dnYAP;NTR)* animals. *Tg(dnYAP;NTR)* froglets (stage 61–66) were heat-shocked, transferred 24 h later for 7 days in a MTZ solution, and finally exposed for 7 more days to BrdU.

(C) Retinal sections from control [*Tg(NTR)*] and *Tg(dnYAP;NTR)* animals, immunostained for rhodopsin and BrdU. Nuclei are counterstained with Hoechst (blue). Note the scattered green staining indicative of photoreceptor degeneration. The number of retinas tested for each condition is indicated on the corresponding bar. Mann-Whitney test, $^{**}p \leq 0.01$. All results are reported as mean ± SEM. Scale bar: 50 μm.

in AAV-YAP5SA-infected retinas. This is reminiscent of the zebrafish situation, where such upregulation occurs in dedifferentiating Müller cells in response to retinal injury (Ramachandran et al., 2010).

Interfering with *Yap* Expression Affects EGFR Signaling in Mouse Reactive Müller Cells

We then sought to identify the molecular mechanisms underlying YAP effect on Müller glia cell-cycle re-entry. Besides cell-cycle genes, our RNA-sequencing (RNA-seq) dataset and pathway analysis also revealed a deregulation of several members of the EGFR pathway in the *Yap* CKO degenerative background (Figures S3A and S3C). Importantly, EGFR signaling is well known for its mitogenic effects on Müller cells during retinal degeneration. Two EGFR ligands, namely EGF or HB-EGF, have in particular been shown to stimulate Müller glia proliferation in zebrafish, chick, or rodents (Close et al., 2006; Karl et al., 2008; Todd et al., 2015; Wan et al., 2012, 2014). As observed with cell-cycle genes, both *Egfr* and two ligand-coding genes (*Hbegf* and *Neuregulin 1*) failed to be properly upregulated upon MNU injection in *Yap* CKO retinas compared with control ones (Figure 6A). Expression of another EGFR-coding gene, *Erbb4* (named also *Her4*), did not appear sensitive to MNU injection in control retinas but was still found significantly decreased in MNU-injected *Yap* CKO mice (Figure 6A). In order to decipher whether these deregulations might be associated with defective EGFR signaling activity, we next assessed the status of the mitogen-activated protein kinase (MAPK) and the phosphatidylinositol 3-kinase (PI3K)/AKT (also known as protein kinase B) pathways, which are known to be required for Müller cell proliferative response to growth factor treatment upon injury (Beach et al., 2017; Ueki and Reh, 2013; Wang et al., 2016). Western blot analysis revealed activation of the extracellular signal-related kinase (ERK) and AKT signaling pathways following MNU injection in control retinas. In the *Yap* CKO context, this increase was significantly attenuated, reflecting lower signaling activation (Figure 6B). Importantly, phosphorylated-ERK (P-ERK) immunostaining confirmed that this decrease was indeed happening in Müller cells: P-ERK labeling (which is barely detectable in non-injured retinas; data not shown) was localized in Müller cell nuclei and processes upon MNU injection and exhibited differential enhancement in control mice (strong signal) compared with *Yap* CKO ones (weaker signal; Figure 6C). Together, these results suggest that YAP is required for proper EGFR signaling through its transcriptional control on both EGFR ligands and receptors. In line with this idea, we found that YAP5SA was sufficient to upregulate *Egfr* expression upon AAV intraocular injections (Figures 6D and 6E). *Hbegf* levels showed a slight trend upward in retinas infected with AAV-YAP5SA, but this did not reach the level of statistical significance. This further supports the idea that YAP regulates the EGFR pathway in Müller glia.

YAP Mitogenic Effects on Müller Cells Requires EGFR Pathway Activity

In order to investigate whether this YAP-EGFR interaction might converge on cell-cycle gene regulation, we attempted to rescue the *Yap* CKO phenotype through EGFR signaling activation. To this aim, we first decided to treat *Yap* CKO explants with HB-EGF, because this EGFR ligand failed to be properly upregulated upon MNU treatment in the absence of YAP and, in contrast, was found increased upon infection with AAV-YAP5SA (Figures 6A and 6E). As expected from our previous observations in MNU and *rd10* mice (Hamon et al., 2017), we found an increase in YAP level accompanying the degenerative process in explants (Figures 7A and 7B). Moreover, as described above with both paradigms (Figures 2D and S4B), this correlated with Cyclin D1 upregulation (Figures 7C and 7D, compare lanes 1 and 2), and this response was impaired in *Yap* CKO explants (Figure 7D,

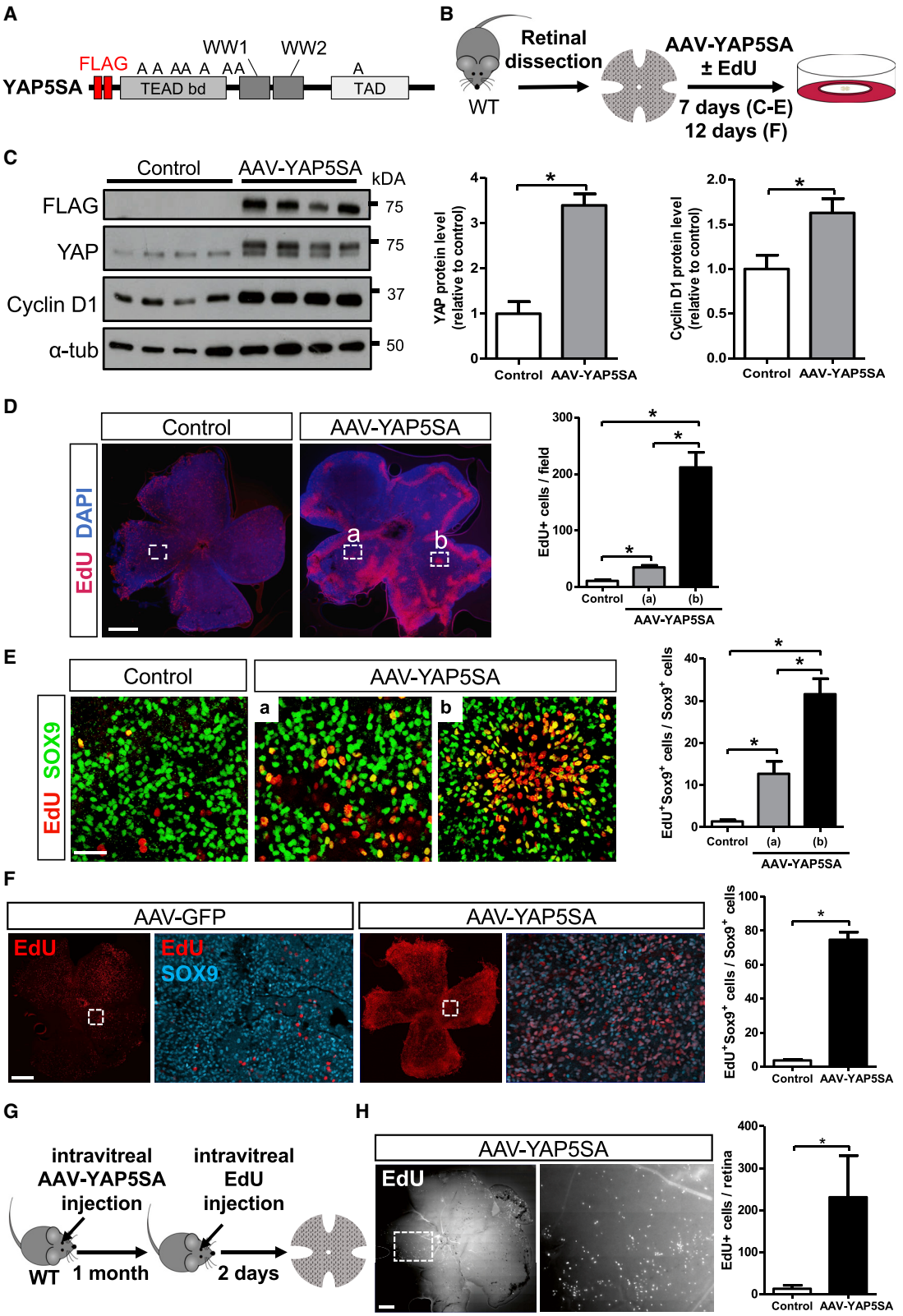

(legend on next page)

compare lanes 2 and 3). Following HB-EGF addition, Cyclin D1 levels were indistinguishable between *Yap* CKO and control explants (Figure 7D, compare lanes 4 and 5). We next attempted an *in vivo* rescue following intravitreal injection of HB-EGF in *Yap* CKO*;rd10* mice. We found that expression of both Cyclin D1 and Cyclin D3 could be restored to the untreated control level (Figures 7E and 7F, compare lanes 2 and 5). Finally, to strengthen the idea of YAP acting upstream the EGFR pathway in Müller glia cell-cycle gene regulation, we assessed whether blocking the EGFR pathway could impair YAP5SA mitogenic effects on Müller glia. We found indeed that pharmacological inhibition of Erk phosphorylation using explant treatment with U0126 (Figures 7G and 7H) dramatically decreased YAP5SA-dependent EdU incorporation in Müller cells (Figure 7I). By demonstrating the EGFR signaling requirement downstream of YAP activity, this result strongly supports a model whereby *in vivo* functional interaction between the two pathways promotes Müller cell proliferative response.

DISCUSSION

Through back-and-forth investigations in both mouse and *Xenopus* retinas, we discovered a pivotal role for YAP in the regulation of Müller cell response to injury. We in particular reveal that YAP triggers their exit from quiescence in a degenerative context. In *Xenopus*, this is accompanied with intense proliferation, but not in mouse. We, however, demonstrate that enhancing YAP activity is sufficient to boost the naturally limited proliferative potential of mammalian Müller glia. In addition, our findings unravel a YAP-EGFR axis in Müller glia cell-cycle reentry that sheds a new light on the genetic network underlying their recruitment following retinal injury.

YAP knockout in several mammalian organs, such as liver, pancreas, intestine, and mammary gland, unexpectedly suggested that this factor is dispensable to maintain normal adult tissue homeostasis (Piccolo et al., 2014). In line with this, we did not observe any major abnormalities in *Yap* CKO retinal morphology and function. We, however, revealed YAP requirement in reactive Müller glia. Reactive gliosis occurs upon retinal stress or injury (Bringmann et al., 2009) and includes a series of characteristic morphological and molecular changes. Importantly, a feature of reactive Müller cells is their exit from a quiescent G0 state. Although their cell cycle rarely reaches S phase, G0 to G1 progression is in particular materialized by the upregulation of genes encoding components of Cyclin D-Cyclin-dependent kinase (CDK) complexes, known to drive early to mid-G1 phase progression (Suga et al., 2014). We found that many cell-cycle genes, including *Ccnd* and *Cdk* genes, are downregulated in *Yap* CKO reactive Müller cells, suggesting that this process is impaired in the absence of YAP. Many different transcription factors have been identified that directly regulate *Ccnd1* promoter (Wang et al., 2004). Remarkably, YAP has been described as one of them in cancer cells (Mizuno et al., 2012). In addition, *Ccnd1* was shown to be activated by YAP overexpression in the chick neural tube (Cao et al., 2008). However, in that study, the authors reported that YAP is not required for its basal transcription. In contrast, we found in Müller cells that YAP is necessary both to maintain basal levels of Cyclin D1 in physiological conditions and for enhancing its expression upon injury. This reinforces the hypothesis that *Ccnd1* may be a direct YAP target gene in Müller glia. This could also be the case for *Cdk6*, as previously reported in a human fibroblastic cell line (Xie et al., 2013). Although our data suggest that YAP functions upstream of the EGFR pathway in the regulation of cell-cycle genes, we thus do not exclude EGFR-independent mechanisms as well.

Although dispensable in several homeostatic contexts, YAP is now well recognized as a central player in the regeneration of diverse tissues in different organisms (Barry and Camargo, 2013). As far as *Xenopus* is concerned, its importance in tissue repair had previously been demonstrated in the context of epimorphic limb and tail regeneration (Hayashi et al., 2014a, 2014b). We here bring new insights to the field by highlighting its requirement for *Xenopus* Müller cell proliferation in a lesioned or degenerative context. In mammals, YAP overexpression or Hippo pathway inhibition was already reported to stimulate regeneration of several injured organs, such as the heart, liver,

Figure 5. YAP Overexpression in Mouse Müller Cells Triggers Their Proliferative Response

(A) Schematic representation of the constitutively active FLAG-tagged YAP5SA construct. The "A" letters indicate the positions of the serine-to-alanine substitutions. TAD, transcription activation domain; TEAD bd, TEAD binding domain; WW1 and WW2, WW domains.

(B) Timeline diagram of the experimental procedure used in (C–F). Retinas from WT mice were flattened, infected with AAV-GFP (control) or AAV-YAP5SA, and cultured for 7 (C–E) or 12 days (F). In (D–F), EdU was added to the culture medium.

(C) Western blot analysis of YAP (using an anti-FLAG or an anti-YAP antibody) and Cyclin D1 expression. α-Tubulin labeling was used to normalize the signal. n = 4 explants for each condition.

(D) EdU labeling on whole flat-mounted retinas, 7 days after AAV infection. Nuclei are counterstained with DAPI (blue). The "b" box corresponds to a region exhibiting a high concentration of EdU-positive cells (~20-fold increase compared with the control), whereas the "a" box shows an area outside such patches (~3-fold increase compared with the control). n = 3 explants for each condition.

(E) Enlargement of the explant regions delineated with white boxes in (D), showing $EdU^+/SOX9^+$ doubled-labeled cells (yellow) in the inner nuclear layer. n = 3 explants for each condition. In AAV-YAP5SA-infected explants, EdU^+ (D) or $EdU^+/SOX9^+$ (E) cells were quantified outside (a) or inside (b) EdU patches.

(F) EdU and Sox9 co-labeling on whole flat-mounted retinas, 12 days after AAV infection. Enlargements show the inner nuclear layer of explant regions delineated with white boxes. n = 3 explants for each condition.

(G) Timeline diagram of the experimental procedure used in (H). WT mice were intravitreally injected with AAV-GFP (control) or AAV-YAP5SA. EdU was administered into the eye 1 month later. Retinas were subsequently flattened and subjected to EdU labeling.

(H) EdU labeling of a flat-mounted retina following *in vivo* infection with AAV-YAP5SA. The enlargement shows the retinal region delineated with the white box. n = 7 (control) or 12 (AAV-YAP5SA) retinas.

Mann-Whitney test, $*p \leq 0.05$. All results are reported as mean ± SEM. Scale bars, 500 μm (D, F, and H); 20 μm (E).

See also Figures S6 and S7.

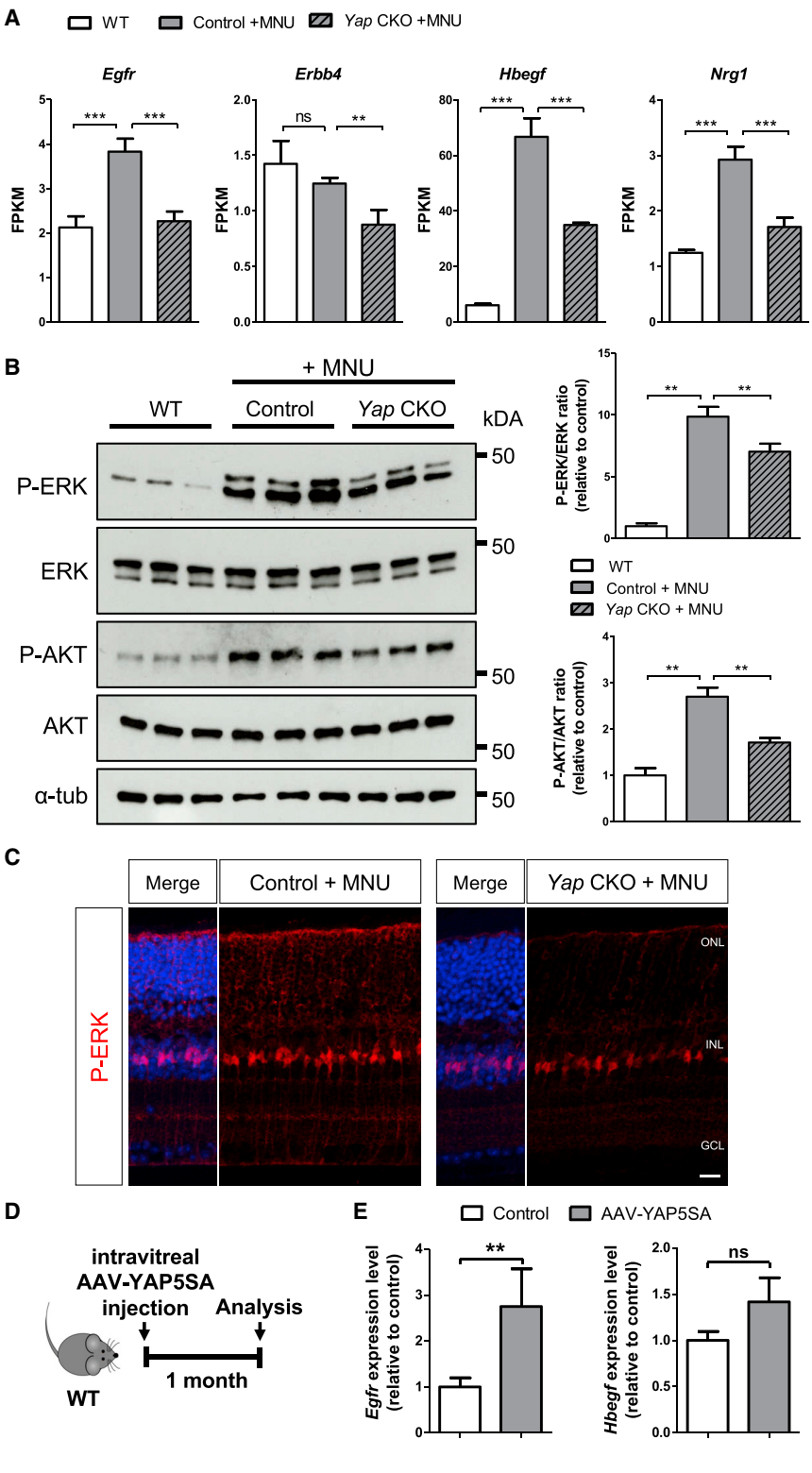

Figure 6. YAP Regulates the Expression of EGFR Signaling Components

(A) Relative RNA expression (in fragments per kilobase of exon per million fragments mapped [FPKM]; data retrieved from the RNA-seq experiment) of *Egfr*, *Erbb4*, *Hbegf*, and *Neuregulin1* (*Nrg1*), in retinas from non-injected WT mice or control and *Yap* CKO mice injected with 4-OHT and MNU as shown in Figure 1F.

(B) Western blot analysis of P-ERK/ERK and P-AKT/AKT ratios on the same experimental conditions. α-Tubulin labeling was used to normalize the signal. n = 6 mice for each condition.

(C) Retinal sections from control and *Yap* CKO mice, immunostained for P-ERK. Nuclei are counterstained with DAPI (blue).

(D) Timeline diagram of the experimental procedure used in (E). WT mice were intravitreally injected with AAV-GFP (control) or AAV-YAP5SA. Retinas were then harvested 1 month later for qPCR analysis.

(E) qRT-PCR analysis of *Hbegf* and *Egfr* expression (10 biological replicates per condition). GCL, ganglion cell layer; INL, inner nuclear layer; ONL, outer nuclear layer.

Mann-Whitney test (except in A where p values were obtained using EdgeR), $*p \leq 0.05$, $**p \leq 0.01$; $***p \leq 0.001$. All results are reported as mean ± SEM. ns, non-significant. Scale bar: 20 μm.

See also Figure S3.

or intestine (Johnson and Halder, 2014; Loforese et al., 2017; Wang et al., 2018). Furthermore, it was recently discovered that YAP/TAZ can act as reprogramming factors, able to turn differentiated cells into their corresponding somatic stem cells (Monroe et al., 2019; Panciera et al., 2016). We here report that enhancing YAP activity awakes quiescent Müller cells and powerfully boosts their proliferative properties both *ex vivo* and *in vivo*. This might be accompanied by their dedifferentiation as inferred from the up-regulation of *Ascl1* expression. Investigating this issue will require assessing whether other retinal progenitor markers are re-expressed in these proliferating Müller cells in order to further characterize their identity. Whether the increased proliferation of YAP-overexpressing Müller cells leads to the production of new neuronal cells will also be an important point to address. Interestingly, following conditional overexpression of YAP5SA, Rueda et al. (2019 [this issue of *Cell Reports*]) confirmed Müller glia cell-cycle re-entry and further showed that a very small subset of reactivated cells may indeed differentiate into neurons. Given YAP efficient mitogenic activity, getting higher rates of differentiation will presumably require (1) controlling its expression in a defined time period using genetic tools allowing for its transient activation (for instance, a doxycycline-inducible construct as previously described) (Panciera et al., 2016); and (2) overexpressing afterward transcription factors known to promote

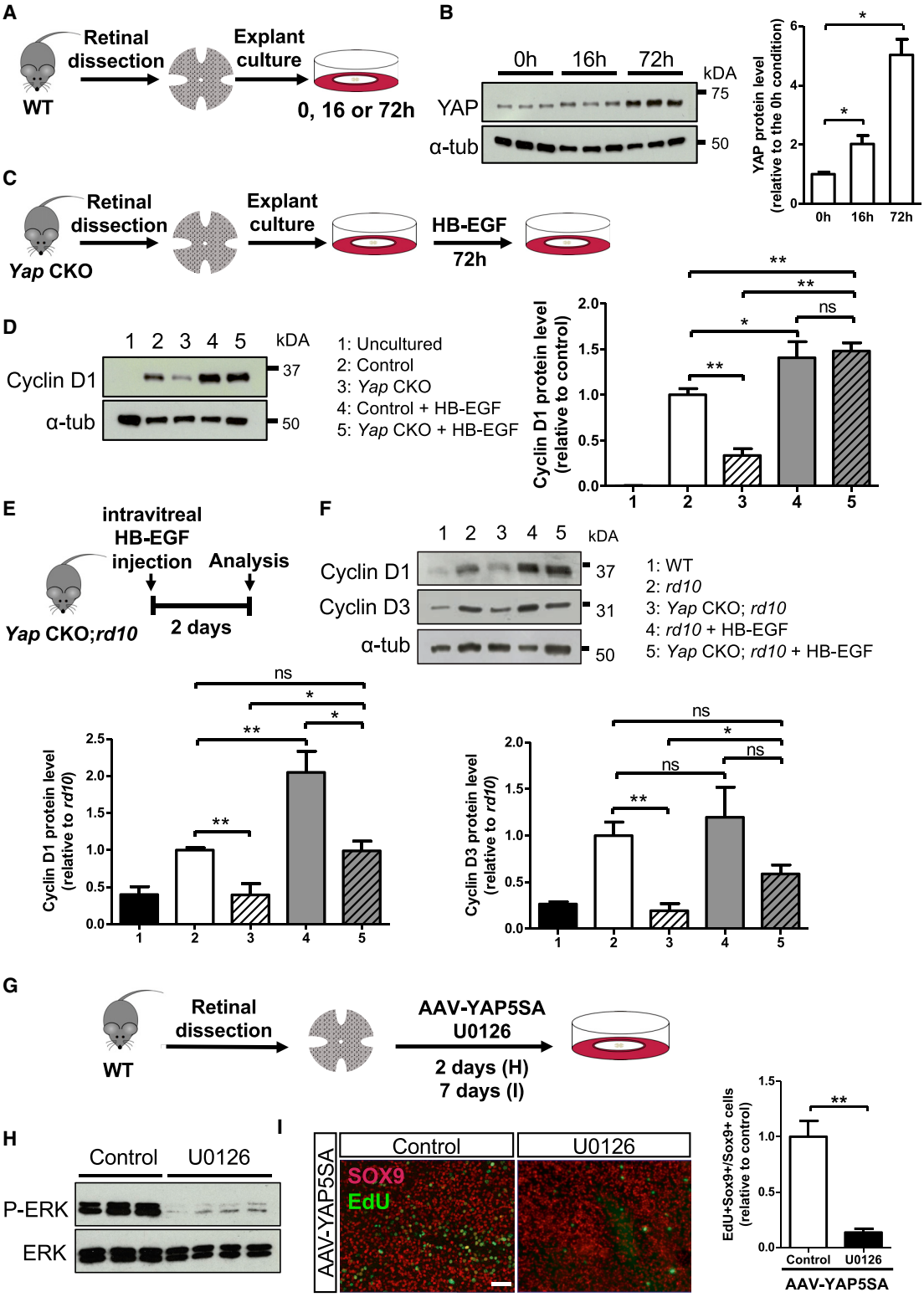

Figure 7. EGFR Signaling Is Required for YAP-Induced Proliferation of Müller Cells

(A) Timeline diagram of the experimental procedure used in (B). Retinas from WT mice were flattened and cultured for 0, 16, or 72 h.

(B) Western blot analysis of YAP expression on retinal explant extracts. α-Tubulin labeling was used to normalize the signal. n = 3 mice for each condition.

(legend continued on next page)

neuronal specification, as reported in a recent study describing Wnt-dependent retinal regeneration (Yao et al., 2018).

YAP is now well recognized as a molecular hub connecting several key signaling pathways (Barry and Camargo, 2013). In animal models harboring retinal regeneration properties such as zebrafish or chick (Hamon et al., 2016; Kaur et al., 2018; Wan and Goldman, 2016), several factors, like Notch, Wnt, or Shh, were shown to regulate Müller cell proliferative response. Given the known interplay between YAP and these pathways in various cellular contexts (Lin et al., 2012; Yu et al., 2015), it would be interesting to seek for their potential functional interactions in *Xenopus* Müller cell-dependent retinal regeneration. In mammals, Hippo/Wnt cross-talks are in particular well documented (Hansen et al., 2015), and Wnt is known to efficiently stimulate Müller cell proliferation following injury (Yao et al., 2018). However, our RNA-seq analysis did not highlight Wnt among the pathways that are deregulated upon *Yap* deletion. In contrast, we here revealed that YAP is required for proper expression and activity of EGFR pathway components in Müller cells following retinal degeneration. Such functional interaction was previously reported in other contexts. The EGFR ligand amphiregulin (AREG) was in particular shown to be regulated by YAP in human mammary epithelial cells or in cervical cancer cells (He et al., 2015a; Zhang et al., 2009). We did not identify *Areg* as deregulated in *Yap* CKO retinas, but we retrieved in our RNA-seq dataset four genes encoding either ligands (HB-EGF and Neuregulin1) or receptors (EGFR and ERBB4) of the pathway. Interestingly, all were reported as direct YAP target genes in human ovarian cells (He et al., 2015b), suggesting that it could be the case in Müller cells as well. Besides, our results demonstrate that EGFR signaling activity is required for YAP mitogenic effects on Müller cells. Considering that EGFR signaling is a key pathway inducing Müller glia cell-cycle re-entry (Close et al., 2005, 2006; Karl et al., 2008; Löffler et al., 2015; Todd et al., 2015; Ueki and Reh, 2013; Wan et al., 2012, 2014), such functional interaction brings YAP at the core of Müller cell reactivation mechanisms. Altogether, we propose the YAP-EGFR axis as a central player in Müller glia response to retinal damage. Interestingly, this is reminiscent of the intestinal regeneration situation, where YAP-dependent EGFR signaling has previously been reported to drive tissue repair upon injury (Gregorieff et al., 2015). Noteworthy, it was reported that EGF-induced proliferation of Müller cells is greatly altered with age, with a proportion of proliferating cells decreasing from 86% at P8 to 9% at P12 following 6 days of explant culture (Löffler et al., 2015). YAP5SA appears much more potent as we estimated the proportion of proliferative Müller cells at about 25% at P30 following 7 days of explant culture. In addition, although EGF can stimulate Müller glia proliferation in a degenerative context, it does not have any mitogenic effect in undamaged chick or mouse retinas (Todd et al., 2015). The same holds true for the proneural transcription factor ASCL1, which promotes Müller cell reprogramming and proliferation following retinal damage, but not in the intact retina (Ueki et al., 2015). Contrasting with these data, we observed that forced YAP5SA expression *in vivo* is sufficient to promote Müller glia cell-cycle re-entry in a non-degenerative context. Altogether, this strongly suggests that YAP not only regulates the EGFR pathway but probably other ones, which results in robust mitogenic stimulation of Müller glia and this even in the uninjured retina.

As a whole, by identifying YAP as a powerful inducer of Müller glia proliferation, our findings open new avenues for research aimed at developing therapeutic strategies based on endogenous repair of the retina.

STAR★METHODS

Detailed methods are provided in the online version of this paper and include the following:

- KEY RESOURCES TABLE
- CONTACT FOR REAGENT AND RESOURCE SHARING
- EXPERIMENTAL MODEL AND SUBJECT DETAILS
  - Mouse lines and degenerative models
  - *Xenopus* lines and regeneration models
- METHOD DETAILS
  - Microinjection in *Xenopus* embryos
  - Mouse retinal explants
  - AAV production and retinal transduction
  - Intravitreal injection
  - Electroretinography
  - Western-blotting
  - Whole transcriptome sequencing and data analysis
  - RNA extraction and RT-qPCR
  - Histology & Immunofluorescence
  - TUNEL assay and EdU labeling
  - Imaging
- QUANTIFICATION AND STATISTICAL ANALYSIS
- DATA AND SOFTWARE AVAILABILITY

(C) Timeline diagram of the experimental procedure used in (D). Retinas from control and *Yap* CKO mice were cultured for 72 h with or without HB-EGF.
(D) Western blot analysis of Cyclin D1 expression on retinal explant extracts. α-Tubulin labeling was used to normalize the signal. n = 3 explants for the uncultured condition; n = 6 explants for all other conditions.
(E) Timeline diagram of the experimental procedure used in (F). WT, *rd10*, or *Yap* CKO;*rd10* mice were intravitreally injected with PBS (control vehicle) or HB-EGF. Retinas were then harvested 2 days later.
(F) Western blot analysis of Cyclin D1 and Cyclin D3 expression on retinal extracts. α-Tubulin labeling was used to normalize the signal. n = 3–5 retinas for each condition.
(G) Timeline diagram of the experimental procedure used in (H) and (I). Retinas from WT mice were flattened, infected with AAV-YAP5SA, and cultured for 2 or 7 days in the presence of U0126 or vehicle (control).
(H) Western blot analysis of pERK and ERK expression. Shown are results from three different explants for each condition.
(I) EdU and Sox9 co-labeling in the inner nuclear layer of retinal explants. n = 6 explants for the control and 5 for the U0126-treated condition.
Mann-Whitney test, *p ≤ 0.05, **p ≤ 0.01. All results are reported as mean ± SEM. ns, non-significant. Scale bar: 50 μm.

SUPPLEMENTAL INFORMATION

Supplemental Information can be found online at https://doi.org/10.1016/j.celrep.2019.04.045.

ACKNOWLEDGMENTS

We are thankful to S. Blackshaw, J. Wrana, and S. Meilhac for mouse lines. We are grateful to E.-K. Grellier and S. Lourdel for their help with the maintenance of mouse colonies. We would also like to thank E.-K. Grellier for performing the ERG recordings; S. Lourdel, S. Lele, K. Parain, C. Borday, and R. Langhe for their technical assistance with *Xenopus* experiments; and C.-J. Simon for her help with mouse intraocular injections. This work has benefited from the facilities and expertise of the high-throughput sequencing core facility of I2BC (Centre de Recherche de Gif; https://www.i2bc.paris-saclay.fr/?lang=fr). This research was supported by grants to M.P. from the FRM, Association Retina France, Fondation Valentin Haüy, UNADEV, and the DIM Région Île de France. A.H. is an Association Retina France and ARC fellow. D.G.-G. is a FRM fellow.

AUTHOR CONTRIBUTIONS

A.H., D.G.-G., D.A., J.B., A.C., and J.E.R. designed and performed the experiments and analyzed the data; D.D. supervised AAV production; M.L. revised the manuscript; M.P. designed the study, analyzed the data, wrote the manuscript with the help of A.H. and D.A., and supervised the study.

DECLARATION OF INTERESTS

The authors declare no competing interests.

Received: October 26, 2018
Revised: February 25, 2019
Accepted: April 9, 2019
Published: May 7, 2019

REFERENCES

Aurnhammer, C., Haase, M., Muether, N., Hausl, M., Rauschhuber, C., Huber, I., Nitschko, H., Busch, U., Sing, A., Ehrhardt, A., and Baiker, A. (2012). Universal real-time PCR for the detection and quantification of adeno-associated virus serotype 2-derived inverted terminal repeat sequences. Hum. Gene Ther. Methods *23*, 18–28.

Azzolin, L., Panciera, T., Soligo, S., Enzo, E., Bicciato, S., Dupont, S., Bresolin, S., Frasson, C., Basso, G., Guzzardo, V., et al. (2014). YAP/TAZ incorporation in the β-catenin destruction complex orchestrates the Wnt response. Cell *158*, 157–170.

Barry, E.R., and Camargo, F.D. (2013). The Hippo superhighway: signaling crossroads converging on the Hippo/Yap pathway in stem cells and development. Curr. Opin. Cell Biol. *25*, 247–253.

Barry, E.R., Morikawa, T., Butler, B.L., Shrestha, K., de la Rosa, R., Yan, K.S., Fuchs, C.S., Magness, S.T., Smits, R., Ogino, S., et al. (2013). Restriction of intestinal stem cell expansion and the regenerative response by YAP. Nature *493*, 106–110.

Beach, K.M., Wang, J., and Otteson, D.C. (2017). Regulation of Stem Cell Properties of Müller Glia by JAK/STAT and MAPK Signaling in the Mammalian Retina. Stem Cells Int. *2017*, 1610691.

Bringmann, A., Pannicke, T., Grosche, J., Francke, M., Wiedemann, P., Skatchkov, S.N., Osborne, N.N., and Reichenbach, A. (2006). Müller cells in the healthy and diseased retina. Prog. Retin. Eye Res. *25*, 397–424.

Bringmann, A., Iandiev, I., Pannicke, T., Wurm, A., Hollborn, M., Wiedemann, P., Osborne, N.N., and Reichenbach, A. (2009). Cellular signaling and factors involved in Müller cell gliosis: neuroprotective and detrimental effects. Prog. Retin. Eye Res. *28*, 423–451.

Cabochette, P., Vega-Lopez, G., Bitard, J., Parain, K., Chemouny, R., Masson, C., Borday, C., Hedderich, M., Henningfeld, K.A., Locker, M., et al. (2015). YAP controls retinal stem cell DNA replication timing and genomic stability. eLife *4*, e08488.

Cao, X., Pfaff, S.L., and Gage, F.H. (2008). YAP regulates neural progenitor cell number via the TEA domain transcription factor. Genes Dev. *22*, 3320–3334.

Chang, B., Hawes, N.L., Pardue, M.T., German, A.M., Hurd, R.E., Davisson, M.T., Nusinowitz, S., Rengarajan, K., Boyd, A.P., Sidney, S.S., et al. (2007). Two mouse retinal degenerations caused by missense mutations in the β-subunit of rod cGMP phosphodiesterase gene. Vision Res. *47*, 624–633.

Chen, Q., Zhang, N., Gray, R.S., Li, H., Ewald, A.J., Zahnow, C.A., and Pan, D. (2014a). A temporal requirement for Hippo signaling in mammary gland differentiation, growth, and tumorigenesis. Genes Dev. *28*, 432–437.

Chen, Y.Y., Liu, S.L., Hu, D.P., Xing, Y.Q., and Shen, Y. (2014b). N -methyl- N -nitrosourea-induced retinal degeneration in mice. Exp. Eye Res. *121*, 102–113.

Choi, V.W., Asokan, A., Haberman, R.A., and Samulski, R.J. (2007). Production of recombinant adeno-associated viral vectors. Curr. Protoc. Hum. Genet. *Chapter 12*, Unit 12.9.

Close, J.L., Gumuscu, B., and Reh, T.A. (2005). Retinal neurons regulate proliferation of postnatal progenitors and Müller glia in the rat retina via TGF beta signaling. Development *132*, 3015–3026.

Close, J.L., Liu, J., Gumuscu, B., and Reh, T.A. (2006). Epidermal growth factor receptor expression regulates proliferation in the postnatal rat retina. Glia *54*, 94–104.

Dyer, M.A., and Cepko, C.L. (2000). Control of Müller glial cell proliferation and activation following retinal injury. Nat. Neurosci. *3*, 873–880.

Finch-Edmondson, M.L., Strauss, R.P., Passman, A.M., Sudol, M., Yeoh, G.C., and Callus, B.A. (2015). TAZ protein accumulation is negatively regulated by YAP abundance in mammalian cells. J. Biol. Chem. *290*, 27928–27938.

Fu, V., Plouffe, S.W., and Guan, K.L. (2017). The Hippo pathway in organ development, homeostasis, and regeneration. Curr. Opin. Cell Biol. *49*, 99–107.

Gee, S.T., Milgram, S.L., Kramer, K.L., Conlon, F.L., and Moody, S.A. (2011). Yes-associated protein 65 (YAP) expands neural progenitors and regulates Pax3 expression in the neural plate border zone. PLoS ONE *6*, e20309.

Gregorieff, A., Liu, Y., Inanlou, M.R., Khomchuk, Y., and Wrana, J.L. (2015). Yap-dependent reprogramming of Lgr5(+) stem cells drives intestinal regeneration and cancer. Nature *526*, 715–718.

Hamon, A., Roger, J.E., Yang, X.J., and Perron, M. (2016). Müller glial cell-dependent regeneration of the neural retina: An overview across vertebrate model systems. Dev. Dyn. *245*, 727–738.

Hamon, A., Masson, C., Bitard, J., Gieser, L., Roger, J.E., and Perron, M. (2017). Retinal Degeneration Triggers the Activation of YAP/TEAD in Reactive Müller Cells. Invest. Ophthalmol. Vis. Sci. *58*, 1941–1953.

Hansen, C.G., Moroishi, T., and Guan, K.L. (2015). YAP and TAZ: a nexus for Hippo signaling and beyond. Trends Cell Biol. *25*, 499–513.

Hayashi, S., Ochi, H., Ogino, H., Kawasumi, A., Kamei, Y., Tamura, K., and Yokoyama, H. (2014a). Transcriptional regulators in the Hippo signaling pathway control organ growth in Xenopus tadpole tail regeneration. Dev. Biol. *396*, 31–41.

Hayashi, S., Tamura, K., and Yokoyama, H. (2014b). Yap1, transcription regulator in the Hippo signaling pathway, is required for Xenopus limb bud regeneration. Dev. Biol. *388*, 57–67.

He, C., Mao, D., Hua, G., Lv, X., Chen, X., Angeletti, P.C., Dong, J., Remmenga, S.W., Rodabaugh, K.J., Zhou, J., et al. (2015a). The Hippo/YAP pathway interacts with EGFR signaling and HPV oncoproteins to regulate cervical cancer progression. EMBO Mol. Med. *7*, 1426–1449.

He, C., Lv, X., Hua, G., Lele, S.M., Remmenga, S., Dong, J., Davis, J.S., and Wang, C. (2015b). YAP forms autocrine loops with the ERBB pathway to regulate ovarian cancer initiation and progression. Oncogene *34*, 6040–6054.

Huang, Z., Hu, J., Pan, J., Wang, Y., Hu, G., Zhou, J., Mei, L., and Xiong, W.C. (2016). YAP stabilizes SMAD1 and promotes BMP2-induced neocortical astrocytic differentiation. Development *143*, 2398–2409.

Johnson, R., and Halder, G. (2014). The two faces of Hippo: targeting the Hippo pathway for regenerative medicine and cancer treatment. Nat. Rev. Drug Discov. *13*, 63–79.

Jorstad, N.L., Wilken, M.S., Grimes, W.N., Wohl, S.G., VandenBosch, L.S., Yoshimatsu, T., Wong, R.O., Rieke, F., and Reh, T.A. (2017). Stimulation of functional neuronal regeneration from Müller glia in adult mice. Nature *548*, 103–107.

Karl, M.O., Hayes, S., Nelson, B.R., Tan, K., Buckingham, B., and Reh, T.A. (2008). Stimulation of neural regeneration in the mouse retina. Proc. Natl. Acad. Sci. USA *105*, 19508–19513.

Kaur, S., Gupta, S., Chaudhary, M., Khursheed, M.A., Mitra, S., Kurup, A.J., and Ramachandran, R. (2018). let-7 MicroRNA-Mediated Regulation of Shh Signaling and the Gene Regulatory Network Is Essential for Retina Regeneration. Cell Rep. *23*, 1409–1423.

Kim, D., Langmead, B., and Salzberg, S.L. (2015). HISAT: a fast spliced aligner with low memory requirements. Nat. Methods *12*, 357–360.

Klimczak, R.R., Koerber, J.T., Dalkara, D., Flannery, J.G., and Schaffer, D.V. (2009). A novel adeno-associated viral variant for efficient and selective intravitreal transduction of rat Müller cells. PLoS ONE *4*, e7467.

Lai, D., Ho, K.C., Hao, Y., and Yang, X. (2011). Taxol resistance in breast cancer cells is mediated by the hippo pathway component TAZ and its downstream transcriptional targets Cyr61 and CTGF. Cancer Res. *71*, 2728–2738.

Langhe, R., Chesneau, A., Colozza, G., Hidalgo, M., Ail, D., Locker, M., and Perron, M. (2017). Müller glial cell reactivation in Xenopus models of retinal degeneration. Glia *65*, 1333–1349.

Liao, Y., Smyth, G.K., and Shi, W. (2014). featureCounts: an efficient general purpose program for assigning sequence reads to genomic features. Bioinformatics *30*, 923–930.

Lin, Y.T., Ding, J.Y., Li, M.Y., Yeh, T.S., Wang, T.W., and Yu, J.Y. (2012). YAP regulates neuronal differentiation through Sonic hedgehog signaling pathway. Exp. Cell Res. *318*, 1877–1888.

Löffler, K., Schäfer, P., Völkner, M., Holdt, T., and Karl, M.O. (2015). Age-dependent Müller glia neurogenic competence in the mouse retina. Glia *63*, 1809–1824.

Loforese, G., Malinka, T., Keogh, A., Baier, F., Simillion, C., Montani, M., Halazonetis, T.D., Candinas, D., and Stroka, D. (2017). Impaired liver regeneration in aged mice can be rescued by silencing Hippo core kinases MST1 and MST2. EMBO Mol. Med. *9*, 46–60.

McLaughlin, M.E., Ehrhart, T.L., Berson, E.L., and Dryja, T.P. (1995). Mutation spectrum of the gene encoding the beta subunit of rod phosphodiesterase among patients with autosomal recessive retinitis pigmentosa. Proc. Natl. Acad. Sci. USA *92*, 3249–3253.

Mizuno, T., Murakami, H., Fujii, M., Ishiguro, F., Tanaka, I., Kondo, Y., Akatsuka, S., Toyokuni, S., Yokoi, K., Osada, H., and Sekido, Y. (2012). YAP induces malignant mesothelioma cell proliferation by upregulating transcription of cell cycle-promoting genes. Oncogene *31*, 5117–5122.

Mo, J.S., Park, H.W., and Guan, K.L. (2014). The Hippo signaling pathway in stem cell biology and cancer. EMBO Rep. *15*, 642–656.

Monroe, T.O., Hill, M.C., Morikawa, Y., Leach, J.P., Heallen, T., Cao, S., Krijger, P.H.L., de Laat, W., Wehrens, X.H.T., Rodney, G.G., and Martin, J.F. (2019). YAP Partially Reprograms Chromatin Accessibility to Directly Induce Adult Cardiogenesis In Vivo. Dev. Cell *48*, 765–779.e7.

Müller, B., Wagner, F., Lorenz, B., and Stieger, K. (2017). Organotypic Cultures of Adult Mouse Retina: Morphologic Changes and Gene Expression. Invest. Ophthalmol. Vis. Sci. *58*, 1930–1940.

Nieuwkoop, P., and Faber, J. (1994). Normal Table of Xenopus laevis, Third Edition (Garland Publishing).

Nishioka, N., Inoue, K., Adachi, K., Kiyonari, H., Ota, M., Ralston, A., Yabuta, N., Hirahara, S., Stephenson, R.O., Ogonuki, N., et al. (2009). The Hippo signaling pathway components Lats and Yap pattern Tead4 activity to distinguish mouse trophectoderm from inner cell mass. Dev. Cell *16*, 398–410.

Pak, T., Yoo, S., Miranda-Angulo, A.L., Wang, H., and Blackshaw, S. (2014). Rax-CreERT2 knock-in mice: a tool for selective and conditional gene deletion in progenitor cells and radial glia of the retina and hypothalamus. PLoS ONE *9*, e90381.

Panciera, T., Azzolin, L., Fujimura, A., Di Biagio, D., Frasson, C., Bresolin, S., Soligo, S., Basso, G., Bicciato, S., Rosato, A., et al. (2016). Induction of Expandable Tissue-Specific Stem/Progenitor Cells through Transient Expression of YAP/TAZ. Cell Stem Cell *19*, 725–737.

Pertea, M., Kim, D., Pertea, G.M., Leek, J.T., and Salzberg, S.L. (2016). Transcript-level expression analysis of RNA-seq experiments with HISAT, StringTie and Ballgown. Nat. Protoc. *11*, 1650–1667.

Piccolo, S., Dupont, S., and Cordenonsi, M. (2014). The biology of YAP/TAZ: hippo signaling and beyond. Physiol. Rev. *94*, 1287–1312.

Ramachandran, R., Fausett, B.V., and Goldman, D. (2010). Ascl1a regulates Müller glia dedifferentiation and retinal regeneration through a Lin-28-dependent, let-7 microRNA signalling pathway. Nat. Cell Biol. *12*, 1101–1107.

Reginensi, A., Scott, R.P., Gregorieff, A., Bagherie-Lachidan, M., Chung, C., Lim, D.S., Pawson, T., Wrana, J., and McNeill, H. (2013). Yap- and Cdc42-dependent nephrogenesis and morphogenesis during mouse kidney development. PLoS Genet. *9*, e1003380.

Robinson, M.D., McCarthy, D.J., and Smyth, G.K. (2010). edgeR: a Bioconductor package for differential expression analysis of digital gene expression data. Bioinformatics *26*, 139–140.

Rueda, E.M., Hall, B.M., Hill, M.C., Swinton, P.G., Tong, X., Martin, J.F., and Poché, R.A. (2019). The Hippo pathway blocks mammalian retinal Müller glial cell reprogramming. Cell Rep. *27*, this issue, 1637–1649.

Sanges, D., Simonte, G., Di Vicino, U., Romo, N., Pinilla, I., Nicolás, M., and Cosma, M.P. (2016). Reprogramming Müller glia via in vivo cell fusion regenerates murine photoreceptors. J. Clin. Invest. *126*, 3104–3116.

Schindelin, J., Arganda-Carreras, I., Frise, E., Kaynig, V., Longair, M., Pietzsch, T., Preibisch, S., Rueden, C., Saalfeld, S., Schmid, B., et al. (2012). Fiji: an open-source platform for biological-image analysis. Nat. Methods *9*, 676–682.

Suga, A., Sadamoto, K., Fujii, M., Mandai, M., and Takahashi, M. (2014). Proliferation potential of Müller glia after retinal damage varies between mouse strains. PLoS ONE *9*, e94556.

Talikka, M., Perez, S.E., and Zimmerman, K. (2002). Distinct patterns of downstream target activation are specified by the helix-loop-helix domain of proneural basic helix-loop-helix transcription factors. Dev. Biol. *247*, 137–148.

Todd, L., Volkov, L.I., Zelinka, C., Squires, N., and Fischer, A.J. (2015). Heparin-binding EGF-like growth factor (HB-EGF) stimulates the proliferation of Müller glia-derived progenitor cells in avian and murine retinas. Mol. Cell. Neurosci. *69*, 54–64.

Ueki, Y., and Reh, T.A. (2013). EGF stimulates Müller glial proliferation via a BMP-dependent mechanism. Glia *61*, 778–789.

Ueki, Y., Wilken, M.S., Cox, K.E., Chipman, L., Jorstad, N., Sternhagen, K., Simic, M., Ullom, K., Nakafuku, M., and Reh, T.A. (2015). Transgenic expression of the proneural transcription factor Ascl1 in Müller glia stimulates retinal regeneration in young mice. Proc. Natl. Acad. Sci. USA *112*, 13717–13722.

Vandesompele, J., De Preter, K., Pattyn, F., Poppe, B., Van Roy, N., De Paepe, A., and Speleman, F. (2002). Accurate normalization of real-time quantitative RT-PCR data by geometric averaging of multiple internal control genes. Genome Biol. *3*, research0034.1–0034.11.

Walter, W., Sánchez-Cabo, F., and Ricote, M. (2015). GOplot: an R package for visually combining expression data with functional analysis. Bioinformatics *31*, 2912–2914.

Wan, J., and Goldman, D. (2016). Retina regeneration in zebrafish. Curr. Opin. Genet. Dev. *40*, 41–47.

Wan, J., Ramachandran, R., and Goldman, D. (2012). HB-EGF is necessary and sufficient for Müller glia dedifferentiation and retina regeneration. Dev. Cell *22*, 334–347.

Wan, J., Zhao, X.F., Vojtek, A., and Goldman, D. (2014). Retinal injury, growth factors, and cytokines converge on β-catenin and pStat3 signaling to stimulate retina regeneration. Cell Rep. *9*, 285–297.

Wang, C., Li, Z., Fu, M., Bouras, T., and Pestell, R.G. (2004). Signal transduction mediated by cyclin D1: from mitogens to cell proliferation: a molecular target with therapeutic potential. Cancer Treat. Res. *119*, 217–237.

Wang, J., He, C., Zhou, T., Huang, Z., Zhou, L., and Liu, X. (2016). NGF increases VEGF expression and promotes cell proliferation via ERK1/2 and AKT signaling in Müller cells. Mol. Vis. *22*, 254–263.

Wang, J., Liu, S., Heallen, T., and Martin, J.F. (2018). The Hippo pathway in the heart: pivotal roles in development, disease, and regeneration. Nat. Rev. Cardiol. *15*, 672–684.

Wilken, M.S., and Reh, T.A. (2016). Retinal regeneration in birds and mice. Curr. Opin. Genet. Dev. *40*, 57–64.

Xie, Q., Chen, J., Feng, H., Peng, S., Adams, U., Bai, Y., Huang, L., Li, J., Huang, J., Meng, S., and Yuan, Z. (2013). YAP/TEAD-mediated transcription controls cellular senescence. Cancer Res. *73*, 3615–3624.

Yao, K., Qiu, S., Wang, Y.V., Park, S.J.H., Mohns, E.J., Mehta, B., Liu, X., Chang, B., Zenisek, D., Crair, M.C., et al. (2018). Restoration of vision after de novo genesis of rod photoreceptors in mammalian retinas. Nature *560*, 484–488.

Yu, F.X., Meng, Z., Plouffe, S.W., and Guan, K.L. (2015). Hippo pathway regulation of gastrointestinal tissues. Annu. Rev. Physiol. *77*, 201–227.

Zhang, J., Ji, J.Y., Yu, M., Overholtzer, M., Smolen, G.A., Wang, R., Brugge, J.S., Dyson, N.J., and Haber, D.A. (2009). YAP-dependent induction of amphiregulin identifies a non-cell-autonomous component of the Hippo pathway. Nat. Cell Biol. *11*, 1444–1450.

Zhang, W., Nandakumar, N., Shi, Y., Manzano, M., Smith, A., Graham, G., Gupta, S., Vietsch, E.E., Laughlin, S.Z., Wadhwa, M., et al. (2014). Downstream of Mutant KRAS, the Transcription Regulator YAP Is Essential for Neoplastic Progression to Pancreatic Ductal Adenocarcinoma. Sci. Signal. *7*, ra42.

Zhao, B., Wei, X., Li, W., Udan, R.S., Yang, Q., Kim, J., Xie, J., Ikenoue, T., Yu, J., Li, L., et al. (2007). Inactivation of YAP oncoprotein by the Hippo pathway is involved in cell contact inhibition and tissue growth control. Genes Dev. *21*, 2747–2761.

STAR★METHODS

KEY RESOURCES TABLE

REAGENT or RESOURCE	SOURCE	IDENTIFIER
Antibodies		
Mouse monoclonal anti-Akt	Sigma-Aldrich	Cat#P2482; RRID: AB_260913
Mouse monoclonal anti-alpha-tubulin	Sigma-Aldrich	Cat#T5168; RRID: AB_477579
Mouse monoclonal anti-alpha-tubulin	Sigma-Aldrich	Cat#T9026; RRID: AB_477593
Rabbit polyclonal anti-arrestin	EMD Millipore	Cat#AB15282; RRID: AB_1163387
Mouse monoclonal anti-Brn3a	Santa Cruz	Cat#Sc-8429; RRID: AB_626765
Rabbit polyclonal anti-calbindin D-28k	Swant	Cat#300; RRID: AB_10000347
Mouse monoclonal anti-calretinin	EMD Millipore	Cat#MAB1568; RRID: AB_94259
Rat monoclonal anti-CD68	Bio-Rad UK	Cat#MCA1957; RRID: AB_322219
Rabbit polyclonal anti-cyclin D1	Abcam	Cat#ab134175; RRID: AB_2750906
Mouse monoclonal anti-cyclin D3	Cell Signaling	Cat#2936; RRID: AB_2070801
Rabbit polyclonal anti-p44/42 MAPK (ERK1/2)	Cell Signaling	Cat#9102; RRID: AB_330744
Rabbit polyclonal anti-FLAG	Cell Signaling	Cat#F7425; RRID: AB_439687
Rabbit polyclonal anti-GFAP	Dako	Cat#Z0334; RRID: AB_10013382
Goat polyclonal anti-GFP	Abcam	Cat#ab6673; RRID: AB_305643
Mouse monoclonal anti-glutamine synthetase	Abcam	Cat#ab64613; RRID: AB_1140869
Peanut anti-Lectin PNA alexa 568 conjugate	Thermo Fisher Scientific	Cat#L32458
Rabbit polyclonal anti-phospho-Akt (Ser473)	Cell Signaling	Cat#9271; RRID: AB_329825
Rabbit polyclonal anti-phospho-p44/42 MAPK (Erk1/2) (Thr202/Tyr204)	Cell Signaling	Cat#4370; RRID: AB_2315112
Rabbit polyclonal anti-Red Fluorescence Protein	Rockland	Cat#600-401-379; RRID: AB_2209751
Mouse monoclonal anti-Rhodopsin	EMD Millipore	Cat#MAB5316; RRID: AB_2156055
Mouse monoclonal anti-Rhodopsin	EMD Millipore	Cat#MABN15; RRID: AB_10807045
Rabbit polyclonal anti-opsin blue	EMD Millipore	Cat#AB5407; RRID: AB_177457
Rabbit polyclonal anti-SOX9	EMD Millipore	Cat#AB5535; RRID: AB_2239761
Rabbit polyclonal anti-TAZ	Abcam	Cat#ab110239
Rabbit polyclonal anti-Vimentin	Santa Cruz	Cat#sc-7557; RRID: AB_793998
Mouse monoclonal anti-YAP	Abcam	Cat#ab56701; RRID: AB_2219140
Rabbit monoclonal anti-YAP	Abcam	Cat#ab52771; RRID: AB_2219141
Goat anti-mouse IgG1, Alexa 488	Thermo Fisher Scientific	Cat#A21121; RRID: AB_141514
Donkey anti-rabbit, Alexa 488	Thermo Fisher Scientific	Cat#A21206; RRID: AB_141708
Goat anti-mouse IgG1, Alexa 555	Thermo Fisher Scientific	Cat#A21127; RRID: AB_141596
Goat anti-mouse IgG2b, Alexa 555	Thermo Fisher Scientific	Cat#A21147; RRID: AB_1500897
Goat anti-mouse IgG2a, Alexa 555	Thermo Fisher Scientific	Cat#A21127; RRID: AB_141596
Donkey anti-rabbit, Alexa 555	Thermo Fisher Scientific	Cat#A31572; RRID: AB_162543
Goat anti-mouse, Alexa 488	Thermo Fisher Scientific	Cat#A11001; RRID: AB_2534069
Goat anti-mouse, Alexa 594	Thermo Fisher Scientific	Cat#A11005; RRID: AB_141372
Goat anti-rat, Alexa 594	Thermo Fisher Scientific	Cat#A11007; RRID: AB_141374
Goat anti-rabbit, Alexa 488	Thermo Fisher Scientific	Cat#A11008; RRID: AB_143165
Goat anti-rabbit, Alexa 594	Thermo Fisher Scientific	Cat#A11012; RRID: AB_141359
Goat anti-mouse IgG HRP conjugate	Sigma-Aldrich	Cat#A4416; RRID: AB_258167
Donkey anti-rabbit IgG HRP conjugate	GE Health	Cat#NA934; RRID: AB_772206

(*Continued on next page*)

Continued

REAGENT or RESOURCE	SOURCE	IDENTIFIER
Bacterial and Virus Strains		
AAV-GFP	Klimczak et al., 2009	N/A
AAV-YAP5SA	This paper	N/A
Chemicals, Peptides, and Recombinant Proteins		
4-hydroxytamoxifen	Sigma-Aldrich	Cat#H6278
Human recombinant HB-EGF	R&D systems	Cat#259-HE
U0126	Abcam	Cat# ab120241
1-Methyl-1-nitrosourea (MNU)	Trinova Biochem	N/A
Metronidazole (MTZ)	Sigma-Aldrich	Cat# M-183
BrdU	Roche	Cat#10280879001
EdU	Thermo Fisher Scientific	Cat# D1756
DAPI	Thermo Fisher Scientific	Cat#62248
Hoechst	Sigma-Aldrich	Cat#H6024
MS-222	Sigma-Aldrich	Cat#A5040-25G
Rompun 2% (Xylasine)	Bayer	N/A
Imalgene 500 (Kétamine)	MERIAL SAS	N/A
Dexamethasone	Sigma-Aldrich	Cat#D4902
Critical Commercial Assays		
RNA 6000 Nano Kit	Agilent Technologies	Cat#5067-1511
TruSeq Stranded mRNA Library Preparation Kit	Illumina	Cat#20020594
RNeasy mini kit	QIAGEN	Cat#74104
NucleoSpin RNA Plus kit	Macherey Nagel	Cat#740984.50
mMessage mMachine kit	Life Technologies	Cat#AM1340
DC Protein Assay	Bio-Rad	Cat# 500-0116
SuperScript II Reverse Transcriptase kit	Thermo Fisher Scientific	Cat#18064-071
SsoFast EvaGreen supermix	Bio-Rad	Cat#172-5204
SYBR select master mix	Thermo Fisher Scientific	Cat#4472908
DeadEnd Fluorometric TUNEL System	Promega	Cat#G3250
Click-iT Plus EdU Alexa Fluor 555 Imaging Kit	Thermo Fisher Scientific	Cat#C10338
Click-iT Plus EdU Alexa Fluor 647 Imaging Kit	Thermo Fisher Scientific	Cat#C10640
Click-iT Plus EdU Alexa Fluor 488 Imaging Kit	Thermo Fisher Scientific	Cat#C10337
Deposited Data		
RNaseq dataset	This paper	GEO: GSE121858
RNaseq dataset	Hamon et al., 2017	GEO: GSE94534
Experimental Models: Organisms/Strains		
Mouse: C57Bl6/J	Jackson Laboratory	N/A
Mouse: B6.CXB1-*Pde6b*^{rd10}/J	Bo Chang; Chang et al., 2007	N/A
Mouse: *Yap*$^{flox/flox}$	Jeff Wrana; Reginensi et al., 2013	N/A
Mouse: *Rax-CreER*^{T2}	Seth Blackshaw; Pak et al., 2014	N/A
Mouse: *Rax-CreER*^{T2}, *R26-CAG-lox-stop-lox-TdTom (Ai9)*	Seth Blackshaw; Pak et al., 2014	N/A
Xenopus laevis: WT	Centre de Ressources Biologiques Xénopes (CRB)	N/A
Xenopus laevis: *Tg(hsp70:dnYap-GFP, cryga:tdTomato)*	UK *Xenopus* resource center ; Hayashi et al., 2014b	N/A
Xenopus laevis: Tg(Rho:GFP-NTR)	Langhe et al., 2017	N/A
Oligonucleotides		
Primers for genotyping, see Table S2		N/A
Primers for RT-qPCR, see Table S2		N/A

(*Continued on next page*)

Continued

REAGENT or RESOURCE	SOURCE	IDENTIFIER
Recombinant DNA		
Plasmid: pCMV-flag-YAP2-5SA	Kun-Liang Guan	Addgene plasmid#27371; RRID: Addgene_27371
Plasmid: pCS2-YapS98A	Cabochette et al., 2015	N/A
Plasmid: pCS2-flag-YapS98A-GR	This paper	N/A
Software and Algorithms		
LabScribe software	iWorx	https://www.iworx.com/research/software/labscribe/
Fiji	National Institutes of Health	https://fiji.sc/
HISAT2 2.1.0 algorithm	Kim et al., 2015; Pertea et al., 2016	N/A
FeatureCounts algorithm	Liao et al., 2014	http://bioinf.wehi.edu.au/featureCounts/
EdgeR algorithm	Robinson et al., 2010	N/A
PANTHER		http://pantherdb.org/
Kyoto Encyclopedia of Genes and Genome	Kanehisa Laboratories	https://www.genome.jp/kegg/
GOplot	Walter et al., 2015	http://wencke.github.io
Zen software	Zeiss	N/A
Photoshop CS4 software	Adobe	N/A
GraphPad Prism 5.01	GraphPad Software	https://www.graphpad.com/

CONTACT FOR REAGENT AND RESOURCE SHARING

Further information and requests for resources and reagents should be directed to and will be fulfilled by the Lead Contact, Muriel Perron (muriel.perron@u-psud.fr).

EXPERIMENTAL MODEL AND SUBJECT DETAILS

All animal experiments have been carried out in accordance with the European Community Council Directive of 22 September 2010 (2010/63/EEC). All animal cares and experimentations were conducted in accordance with institutional guidelines, under the institutional license D 91-272-105 for mice and the institutional license C 91-471-102 for *Xenopus*. The study protocols were approved by the institutional animal care committee CEEA n°59 and received an authorization by the ''Ministère de l'Education Nationale, de l'Enseignement Supérieur et de la Recherche'' under the reference APAFIS#1018-2016072611404304v1 for mice experiments and APAFIS#998-2015062510022908v2 for *Xenopus* experiments.

Mouse lines and degenerative models

Mice were kept at 21°C, under a 12-hour light/12-hour dark cycle, with food and water supplied *ad libitum*. *Yap*$^{flox/flox}$ mice were obtained from Jeff Wrana's lab (Reginensi et al., 2013) and crossed with heterozygous *Rax-CreER*^{T2} knock-in mice or double heterozygous *Rax-CreER*^{T2}, *R26-CAG-lox-stop-lox-TdTom (Ai9)* mice from Seth Blackshaw's lab (Pak et al., 2014) to generate *Yap*$^{flox/flox}$;*Rax-CreER*^{T2} (*Yap CKO*) and *Yap*$^{flox/flox}$;*Rax-CreER*^{T2};*Ai9* (*Yap CKO; Ai9*) mice. Primer sequences used for genotyping tail snip genomic DNA are provided in Table S2. Cre activity was induced through a single intraperitoneal injection of 4-hydroxytamoxifen (4-OHT; 1 mg) at P10, as previously described (Pak et al., 2014). To generate the *Yap*$^{flox/flox}$;*Rax-CreER*^{T2};*rd10* line (*Yap CKO; rd10*), *Yap*$^{flox/flox}$;*Rax-CreER*^{T2} mice were crossed with homozygous *rd10* mice (*Pde6b*^{rd10}; a model of retinitis pigmentosa, with a mutation in *phosphodiesterase-6b* (*Pde6b*) gene (Chang et al., 2007); The Jackson Laboratory, Bar Harbor, ME, USA). Chemically-induced retinal degeneration was performed through a single intraperitoneal injection of 1-Methyl-1-nitrosourea (MNU, Trinova Biochem) at 60 mg/kg body weight, as previously described (Hamon et al., 2017). All experiments involving adult mice were performed with male or female mice that were 3 to 8 weeks. No difference between sexes was observed in any retinal phenotype.

Xenopus lines and regeneration models

Xenopus laevis tadpoles were obtained by conventional procedures of *in vitro* or natural fertilization, staged according to Nieuwkoop and Faber method (Nieuwkoop and Faber, 1994) and raised at 18-20°C. Heat-shock-inducible dominant-negative YAP transgenic line *Tg(hsp70:dnYap-GFP, cryga:tdTomato)* (Hayashi et al., 2014b) (*Tg(dnYAP)*) was obtained from the UK *Xenopus* resource center (EXRC). Heat-shock-mediated dnYAP expression was induced by shifting the animals from 18-20°C to 34°C for 30 min as previously described (Hayashi et al., 2014b). The transgenic *Xenopus* line *Tg(Rho:GFP-NTR)* (*Tg(NTR)*) used for conditional rod ablation was

generated in the lab and previously described (Langhe et al., 2017). Photoreceptor degeneration was induced by bathing the froglets in a 10 mM MTZ (Sigma-Aldrich) solution for 1 week (Langhe et al., 2017). Retinal mechanical injury was performed as previously described (Langhe et al., 2017), by poking the retina once under a stereomicroscope with a needle (Austerlitz Insect Pins, 0.2 mm), without damaging the cornea or the lens. For cell proliferation assays, *Xenopus* tadpoles (i.e., pre-metamorphic individuals) or froglets (i.e., post-metamorphic individuals) were immersed in a solution containing 1 mM BrdU (5′-bromo-2′-deoxyuridine, Roche) for 3 days or 1 week, as indicated. The solution was renewed every other day.

METHOD DETAILS

Microinjection in *Xenopus* embryos

The *Xenopus* construct *YapS98A,* encoding a constitutively active YAP protein (Ser-98 residue substituted with an alanine), was provided by S Gee and S Moody (Gee et al., 2011) and subcloned into pCS2^{+} (pCS2-*YapS98A*) (Cabochette et al., 2015). A glucocorticoid-inducible FLAG-tagged version of YAPS98A (YAPS98A-GR) was then generated by subcloning in frame the *YapS98A* coding sequence from pCS2-*YapS98A* plasmid into the EcoRI and XhoI sites of pCS2-*flag-GR* (Talikka et al., 2002) (pCS2-*flag-YapS98A-GR*). Following *in vitro* transcription (mMessage mMachine kit, Life Technologies), 200 pg of mRNA were injected at the one-cell stage. *LacZ* mRNAs were injected as controls. Activity of the chimeric YAPS98A-GR protein was induced by addition of 4 mg/ml dexamethasone (dex, Sigma-Aldrich) into the embryo rearing medium.

Mouse retinal explants

Retinas from enucleated P30 eyes were dissected in Hanks' Balanced Salt solution (GIBCO) by removing the anterior segment, vitreous body, sclera and RPE. They were then flat-mounted onto a microporous membrane (13 mm in diameter; Merk Millipore) in a twelve-well culture plate, with the ganglion cell layer facing upward. Each well contained 700 μL of culture medium, consisting in DMEM-Glutamax (GIBCO) supplemented with 1% FBS, 0.6% D-Glucose, 0.2% $NaHCO_3$, 5mM HEPES, 1% B27, 1% N2, 1X Penicillin-Streptomycin. Culture medium containing 100 ng/mL human recombinant HB-EGF (R&D systems), 10 μM of U0126 (Abcam) or vehicle was added from the beginning of the explant culture. Explants were maintained at 37°C in a humidified incubator with 5% CO_2. Half of the culture medium was changed daily. For proliferation assays, 20 mM EdU was applied 7 or 12 days before fixation.

AAV production and retinal transduction

Human YAP5SA cDNA was amplified by PCR from pCMV-flag-YAP2-5SA plasmid (a gift from Kunliang Guan, Addgene plasmid#27371; http://addgene.org/27371; RRID:Addgene_27371) and subcloned into an AAV transfer plasmid, where the expression is driven by the minimal cytomegalovirus (CMV) promoter (Klimczak et al., 2009). AAV vectors were produced as already described using the co-transfection method and purified by iodixanol gradient ultracentrifugation (Choi et al., 2007). AAV vector stocks were tittered by qPCR using SYBR Green (Thermo Fisher Scientific) (Aurnhammer et al., 2012). The previously engineered AAV-GFP (Klimczak et al., 2009) was used as a control. 10^{11} vg of AAV-GFP or AAV-YAP5SA were applied on mouse retinal explants for viral transduction. Infected explants were cultured for 7 or 12 days as indicated before further western blot analysis or EdU labeling.

Intravitreal injection

Mice were first anesthetized through intraperitoneal injection of ketamine (90 mg/ kg, Merial) and xylazine (8 mg/kg, Bayer). They were then topically administered tropicamide (0.5%) and phenylephrine (2.5%) for pupillary dilation. While applying gentle pressure around the eye socket to extrude the eye, a 30-gauge needle was passed through the sclera just behind the limbus, into the vitreous cavity. Injection of 2 μl of AAV (10^{13} vg/ml) or 1 μl of 100 μg/mL HB-EGF (R&D systems) or 1 μl of 1 μg/μl EdU (Thermo Fisher Scientific) was made with direct observation of the needle in the center of the vitreous cavity.

Electroretinography

Electroretinograms (ERGs) were recorded using a Micron IV focal ERG system (Phoenix Research Labs). Mice were dark-adapted overnight, prepared for recording in darkness under dim-red illumination and finally anesthetized as described above. Flash ERG recordings were obtained from one eye. ERG responses were recorded using increasing light intensities ranging from −1.7 to 2.2 log cd·s/m^2 under dark-adapted conditions, and from −0.5 to 2.8 log cd·s/m^2 under a background light that saturates rod function. The interval between flashes varied from 0.7 s at the lowest stimulus strength to 15 s at the highest one. Five to thirty responses were averaged depending on flash intensity. Analysis of a-wave and b-wave amplitudes was performed using LabScribeERG software. The a-wave amplitude was measured from the baseline to the negative peak and the b-wave was measured from the baseline to the maximum positive peak.

Western-blotting

Each protein extract was obtained from a single retina, quickly isolated and frozen at −80°C. Retinas were then lysed in P300 buffer (20 mM Na_2HPO_4; 250 mM NaCl; 30 mM NaPPi; 0.1% Nonidet P-40; 5 mM EDTA; 5mM DTT) supplemented with protease inhibitor

cocktail (Sigma-Aldrich). Lysate concentration was determined using the Lowry protein assay kit (DC Protein Assay; Bio-Rad) and 20 μg/lane of each sample were loaded for western-blot analysis. Between 3 and 6 individuals were tested per condition. Primary/secondary antibodies and their corresponding working dilutions are listed in Table S3. Protein detection was performed using an enhanced chemiluminescence kit (Bio-Rad). Each sample was probed once with anti-α-tubulin antibody for normalization. Quantification was done using Fiji software (National Institutes of Health) (Schindelin et al., 2012).

Whole transcriptome sequencing and data analysis

Whole transcriptome analysis was performed on three independent biological replicates from MNU-injected control and MNU-injected *Yap* CKO retinas at P60 and compared to WT dataset previously published (Hamon et al., 2017) (GEO accession number GSE94534). After harvesting, both retinas for each animal were immediately frozen. RNA was extracted using Nucleospin RNA Plus kit (Macherey-Nagel). RNA quality and quantity were evaluated using a BioAnalyzer 2100 with RNA 6000 Nano Kit (Agilent Technologies). Stranded RNA-Seq libraries were constructed from 100 ng high-quality total RNA (RIN > 8) using the TruSeq Stranded mRNA Library Preparation Kit (Illumina). Paired-end sequencing of 40 bases length was performed on a NextSeq 500 system (Illumina). Pass-filtered reads were mapped using HISAT2 2.1.0 and aligned to mouse reference genome GRCm38 (Kim et al., 2015; Pertea et al., 2016). Count table of the gene features was obtained using FeatureCounts (Liao et al., 2014). Normalization, differential expression analysis and FPKM (fragments per kilobase of exon per million fragments mapped) values were computed using EdgeR (Robinson et al., 2010). An FPKM filtering cutoff of 1 in at least one of the 6 samples was applied. A *p value* of less than or equal to 0.05 was considered significant and a fold change cutoff of 1.5 was applied to identify differentially expressed genes. GO annotation was obtained using PANTHER classification system and pathways analysis was done using the Kyoto Encyclopedia of Genes and Genome (KEGG). Data visualization was done using GOplot R package (Walter et al., 2015).

RNA extraction and RT-qPCR

Total RNA was extracted from mouse neural retina or whole *Xenopus* tadpoles using RNeasy mini kit (QIAGEN) or NucleoSpin RNA Plus kit (Macherey Nagel), respectively. RNA concentration was assessed using the NanoDrop 2000c UV-Vis spectrophotometer (Thermo Fisher Scientific). Total RNA was reverse transcribed in the presence of oligo-(dT)20 using Superscript II reagents (Thermo Fisher Scientific). For each RT-qPCR reaction, 1.5 ng of cDNA was used in triplicates in the presence of EvaGreen (Bio-Rad) on a CFX96 Real-Time PCR Detection System (Bio-Rad). Differential expression analysis was performed using the ΔΔCt method using the geometric mean of *Rps26, Srp72* and *Tbp* as endogenous controls (Vandesompele et al., 2002) for mouse genes, and of *Rpl8* and *Odc1* as endogenous controls for *Xenopus* genes. Relative expression of each gene in each sample was calculated using the mean of the controls as the reference (1 a.u.). Primers are listed in Table S2. RT-qPCR experiments were performed on at least 5 mice or 3 tadpoles per condition, allowing for statistical analysis.

Histology & Immunofluorescence

Pre- and post- metamorphic *Xenopus* individuals were anesthetized in 0.4% MS222 (Sigma-Aldrich) and then fixed in 1X PBS, 4% paraformaldehyde, overnight at 4°C. For mice, the eyes of sacrificed animals were rapidly enucleated and dissected in Hanks' Balanced Salt solution (GIBCO) to obtain posterior segment eye-cups, which were then fixed in 1X PBS, 4% paraformaldehyde for 1 hr at 4°C. Fixed samples were dehydrated, embedded in paraffin and sectioned (7μm) with a Microm HM 340E microtome (Thermo Scientific). Fixed retinal explants were sectioned (7μm) with a Microm HM550 cryostat (Thermo Scientific), following embedment in 1X PBS, 7,5% gelatin, 10% sucrose. Immunostaining on retinal sections or whole explants was performed using standard procedures with the following specificities: (i) An antigen unmasking treatment was done in boiling heat-mediated antigen retrieval buffer (10 mM sodium citrate, pH 6.0) for 20 min; (ii) For *Xenopus* sections, this was followed by a 45 min treatment in 2N HCl at room temperature; (iii) Incubation timing was increased at all steps for immunolabelling on retinal explants. Primary/secondary antibodies and their corresponding working dilutions are listed in Table S3. Nuclei were counterstained with 1μg/ml DAPI (Thermo Fisher Scientific) or Hoechst (Sigma-Aldrich). H&E staining was performed using standard procedure.

TUNEL assay and EdU labeling

Detection of apoptotic cells was conducted on retinal sections using DeadEnd Fluorometric TUNEL System (Promega) according to the manufacturer's instructions. EdU incorporation was detected using the Click-iT EdU Imaging Kit (Thermo Fisher Scientific) following the manufacturer's recommendations. Coverslips were mounted using Fluorsave Reagent (Millipore, USA).

Imaging

Fluorescence and brightfield images were acquired using an ApoTome-equipped AxioImager.M2 microscope or a Zeiss LSM710 confocal microscope. Whole retinal explants were imaged using an AxioZoom.v16 (Zeiss). Image mosaics of whole explants or flat mounted retinas were acquired and combined by the stitching processing method using ZEN Tiles module (Zeiss). Images were processed using Zen (Zeiss), Fiji (National Institutes of Health) and Photoshop CS4 (Adobe) softwares. The same magnification, laser intensity, gain and offset settings were used across animals for any given marker.

QUANTIFICATION AND STATISTICAL ANALYSIS

Quantifications in *Xenopus*: all labeled cells were counted manually. 3 to 10 sections were analyzed for each retina, and an average number was calculated from at least 5 retinas. BrdU-positive cells were counted within the *Xenopus* neural retina (after exclusion of the ciliary marginal zone). The size of dissected *Xenopus* eyes was estimated by measuring the surface of the corresponding pictures using Photoshop CS4 (Adobe) software. Quantifications in mouse: mean number of labeled cells in mouse retinal explants were calculated from 3 different fields of 10^4 μm^2 per retina and using 3 explants per condition (for quantifications on whole explants) or from one field of 10^4 μm^2 per section and using minimum 3 different retinas per condition (for quantifications on explant sections). SOX9-positive mouse Müller cells in Figure 1 were quantified by considering one entire retinal section from 3 different mice for each condition. Statistical analysis was performed with GraphPad Prism 5.01 (GraphPad Software, La Jolla California USA) using the non-parametric Mann-Whitney test in all experiments, except ERG, for which we applied a two-way ANOVA test. p value ≤ 0.05 was considered significant. All results are reported as mean ± SEM.

DATA AND SOFTWARE AVAILABILITY

RNaseq dataset from MNU-injected control and MNU-injected *Yap* CKO retinas has been deposited at the Gene Expression Omnibus under the ID code GEO: GSE121858.